



Innovative Applications of O.R.

## Bayesian sequential data collection for stochastic simulation calibration

Bo Wang<sup>a</sup>, Qiong Zhang<sup>b</sup>, Wei Xie<sup>a,\*</sup><sup>a</sup> Mechanical and Industrial Engineering, Northeastern University, 360 Huntington Avenue, 334 SN, Boston, MA 02115, USA<sup>b</sup> School of Mathematical and Statistical Sciences, Clemson University, O-110 Martin Hall, Clemson, SC 29631, USA

### ARTICLE INFO

#### Article history:

Received 18 December 2017

Accepted 31 January 2019

Available online 13 February 2019

#### Keywords:

Simulation

Calibration

Sequential experiment design

Detailed sample paths

Bayesian method

### ABSTRACT

Simulation is often used to guide the decision making for real complex stochastic systems. To faithfully assess the mean performance of the real system, it is necessary to efficiently calibrate the simulation model. Existing calibration approaches are typically built on the summary statistics of simulation outputs and ignore the serial dependence of detailed output sample paths. Given a tight simulation budget, we develop a Bayesian sequential data collection approach for simulation calibration via exploring the detailed simulation outputs. Then, the calibrated simulation model can be used to guide decision making. Both theoretical and empirical studies demonstrate that we can efficiently use the simulation resources and achieve better calibration accuracy by exploring the first two moment dynamic information of simulation output sample paths.

© 2019 Elsevier B.V. All rights reserved.

### 1. Introduction

Stochastic simulation has been widely used to assess the performance of real complex systems in many applications, such as semiconductor manufacturing and global supply chains. To provide a reliable guidance on decision making, the simulation model needs to be calibrated to match the performance of the real system. In this paper, we focus on the system steady-state mean performance.

The model risk of a simulation model can be induced by the logic approximation and the input model estimation uncertainty. When the real system is very complex and/or some detail information of the system logic may not be available, a simplified simulation model is often used to guide decision making. For example, the semiconductor production processes involve thousands of steps and they are subject to unpredictable disruption, such as breakdowns of key equipments. A simulation model built on a simplified queuing network is often used to guide the production scheduling; see for example Horiguchi, Raghavan, Uzsoy, and Venkateswaran (2001). Since a few work stations with either expensive or unreliable equipments tend to dominate the flow of orders, the production process can be simplified by modeling each bottleneck or near-bottleneck work station and aggregating the remaining stations. Moreover, in many situations, we only record the output

data without collecting the real-world data for some input models, defined as stochastic processes used to drive the simulation experiments (Nelson, 2016). Thus, simulation calibration is often referred to as the procedure of matching the mean responses of real and simulation systems by adjusting unknown parameters of simulation model. These parameters are also known as calibration parameters, see Goeva, Lam, and Zhang (2014) and Plumlee and Lam (2016b).

One brute-force way is to run simulation experiments under different calibration parameter settings, and manually choose the one that provides the optimal match with the historical output data from real systems. However, in the current inter-connected world, decision makers are often facing large-scale stochastic systems. As the system complexity increases, each simulation run could be computationally expensive, and also the dimension of calibration parameters increases. It becomes almost impossible to manually tune the calibration parameters. Moreover, the real-world systems are often required to evolve rapidly in order to remain competitive (Nelson, 2016). To keep the simulation model faithfully representing the fast evolving real system, the calibration parameter setting must be adjusted timely to meet the emerging requirements of decision making. Therefore, in this paper, we develop a Bayesian approach that can efficiently employ the simulation resource to calibrate simulation model, and also automatically provide statistical inference for calibration parameters and system mean response.

Statistical inference for calibration has been developed under both Bayesian and frequentist perspectives with motivation

\* Corresponding author.

E-mail addresses: [wang.bo2@husky.neu.edu](mailto:wang.bo2@husky.neu.edu) (B. Wang), [qiongzc@clemson.edu](mailto:qiongzc@clemson.edu) (Q. Zhang), [w.xie@northeastern.edu](mailto:w.xie@northeastern.edu) (W. Xie).

originally from deterministic computer models. From a Bayesian perspective, the milestone study, [Kennedy and O'Hagan \(2001\)](#), develops a Bayesian framework to predict the real system performance using calibrated computer models. It has been extended to calibrating the mean response of stochastic simulation in recent years; see for example [Yuan, Ng, and Tsui \(2013\)](#). On the other hand, [Tuo and Wu \(2015\)](#) and [Wong, Storlie, and Lee \(2017\)](#) examine statistical inference on the optimal calibration setting of computer model from a frequentist perspective.

In many calibration studies, data from simulation models and real system is given a priori. However, from a simulation practitioners' viewpoint, it is more efficient to calibrate simulation models under a sequential manner: statistical inferences guide the allocation of simulation resource and newly collected simulation data are used to further enhance statistical inference for calibration. Therefore, it is desired to fully combine statistical inference and simulation budget allocation into a sequential procedure for simulation calibration. [Ryzhov \(2018\)](#) makes inroads on developing a sequential data collection method for calibration, called *the local time method*. To enable theoretical investigation of the proposed sequential method, [Ryzhov \(2018\)](#) assumes that the mean performances of different candidate settings have independent normal priors.

Existing approaches, e.g., [Yuan et al. \(2013\)](#) and [Ryzhov \(2018\)](#), only use the summary statistics of simulation output, and ignore the serial dependence carried by the detailed sample paths. In this paper, we explore the detailed output sample paths, utilize the first two moments of serial outputs, and develop a sequential calibration approach that can efficiently employ the simulation resources to improve the calibration accuracy. When lack of real-world input data, identification of underlying input models through calibration, such as the service rates of key working stations in complex semiconductor production processes, provides the insights of system underlying operating status. In addition, given a tight simulation budget, we want to select a simulation model that can accurately predict the real system mean performance. Thus, we use the probability of correct selection (PCS) and expected opportunity cost (EOC) to evaluate the calibration performance. Given a finite simulation budget, both theoretical and empirical studies demonstrate that our calibration approach can deliver better performance than the existing methods based on summary statistics. After that, the calibrated simulation model can be used to guide the decision making. Some preliminary insights of this paper have been reported in our conference paper ([Wang, Zhang, & Xie, 2017](#)).

In sum, the main contributions of our study are described as follows: (1) we explore the detailed output sample paths and propose a sequential data collection approach for stochastic simulation calibration; (2) based on the proposed simulation calibration approach, we further develop a sequential data collection framework to simultaneously calibrate the simulation model and search for the optimal decision; (3) given finite computational resources, our theoretical study and empirical experiments demonstrate that the proposed approach can improve the accuracy of mean performance calibration.

The remaining of this article is organized as follows. In [Section 2](#), we provide a literature review on related topics. [Section 3](#) provides the formal problem description. [Section 4](#) introduces a new sequential calibration approach exploring detailed output sample paths. Under the GP assumption of output sample paths, our theoretical study shows that the proposed approach can lead to better PCS and EOC than the calibration approach built on the summary statistics. In [Section 5](#), we develop the framework that incorporates decision making with calibration in sequential manner. In [Section 6](#), single server queues and a queueing network example are used to study the finite sample performance of our proposal. We conclude this paper in [Section 7](#).

## 2. Literature review

### 2.1. Deterministic simulation calibration

Deterministic simulation calibration has been developed under both Bayesian and frequentist streams. In the Bayesian stream, computer model calibration is often built on the framework introduced by [Kennedy and O'Hagan \(2001\)](#), which provides Bayesian inference for computer model discrepancy and real system responses. It models the unknown response surface of the computer model and the model discrepancy with GPs. Given the data collected from the real and simulation systems, the posterior distribution of calibration parameters is developed to characterize beliefs about the optimal calibration setting, and the posterior predictive distribution is used to quantify the overall prediction uncertainty of the real system response. Some follow-up studies, e.g. [Gramacy et al. \(2015\)](#), [Plumlee \(2017\)](#), improve this framework from various aspects. Frequentist approaches (e.g., [Tuo & Wu, 2016](#); [Tuo & Wu, 2015](#); [Wong et al., 2017](#)) often aim to identify the optimal calibration parameter setting through minimizing distance measures between the computer model and real system outputs. For example, [Tuo and Wu \(2015\)](#) develop an  $L_2$  calibration approach by minimizing the  $L_2$  distance between the physical response surface and the computer outputs.

### 2.2. Stochastic simulation calibration

Several papers focus on stochastic simulation calibration. Some works directly extend the calibration framework for deterministic computer model in [Kennedy and O'Hagan \(2001\)](#) by replacing the deterministic computer model output with the stochastic mean performance adding a simulation error term; see [Yuan et al. \(2013\)](#) and [Yuan and Ng \(2013\)](#) for example. Different types of calibration frameworks have also been developed for stochastic simulation. [Goeva et al. \(2014\)](#) study the problem of estimating input models in stochastic simulation with only the availability of the output data. [Plumlee and Lam \(2016b\)](#) consider learning the probability distribution of the discretized model response, and develop statistical inference approaches for model discrepancy under this discretized response.

### 2.3. Sequential data collection

Under the assumption that the calibration parameter space can be discretized to a finite number of candidates, sequential data collection for optimizing calibration parameter setting is closely related to ranking and selection in the literature of simulation optimization; see [Frazier, Powell, and Dayanik \(2008\)](#), [Ryzhov \(2016\)](#), and [Scott, Frazier, and Powell \(2011\)](#) for example. In addition, E-type (Expected Improvement) sequential data collection methods have been further developed for simulation calibration problems, e.g., [Frazier, Powell, and Simao \(2009\)](#) and [Ryzhov \(2018\)](#). [Frazier et al. \(2009\)](#) consider calibrating an approximate dynamic programming (ADP) model with the knowledge-gradient algorithm. [Ryzhov \(2018\)](#) develops a sequential data collection framework for simulation calibration, where the *local time method* is proposed to select new simulation runs to maximize the improvement of calibration accuracy.

### 2.4. Simulation analytics

We close this section by briefly reviewing literatures on simulation analytics and output analysis that explore the detailed simulation output. Traditional simulation study, as well as calibration approaches, are typically based on the summary statistics of the simulation outputs, e.g., the sample mean of customer

waiting times in an  $M/M/1$  queue, and ignore the detailed information from the simulation sample path outputs. Since the advances in data storage and computing makes it easy to generate and save the comprehensive data of the output (Nelson, 2016), some recent works on simulation output analysis (e.g., Plumlee & Lam, 2016a) and simulation analytics (e.g., Lin & Nelson, 2016) exploit the simulation output sample paths to support decision making and system diagnostics.

### 3. Problem description

Let  $\mu^p(\mathbf{x})$  be the mean performance of the real physical system under decision  $\mathbf{x} \in \mathcal{X}$ , where  $\mathcal{X}$  is the decision space. The problem is to find the optimal decision maximizing the mean performance

$$\mathbf{x}^* \in \operatorname{argmax}_{\mathbf{x} \in \mathcal{X}} \mu^p(\mathbf{x}). \quad (1)$$

Without an explicit form of real system mean response surface  $\mu^p(\mathbf{x})$ , this problem can be solved via the ranking and selection approaches (Powell & Ryzhov, 2012). However, ranking and selection requires running experiments extensively on the physical system, which is often expensive or prohibitive in practice. Alternatively, we could guide the decision making by using the simulation model. To provide reliable guidance, we require that the performance of simulation model matches well with that of the physical system. This procedure is often called *simulation calibration*.

Simulation models are constructed to mimic the physical system based on domain knowledge. We denote the mean performance of the simulation model by  $\mu(\mathbf{x}, \theta)$ , where the calibration setting  $\theta$  is a point in the space  $\Theta$ . We adjust  $\theta \in \Theta$ , and find the optimal parameter setting, denoted by  $\theta^*$ , such that  $\mu(\mathbf{x}, \theta^*)$  matches well with  $\mu^p(\mathbf{x})$  over the entire decision space  $\mathcal{X}$ . Following the  $L_2$  distance calibration proposed by Tuo and Wu (2015), the optimal calibration parameter setting is defined by

$$\theta^* \in \operatorname{argmin}_{\theta \in \Theta} \int_{\mathcal{X}} [\mu^p(\mathbf{x}) - \mu(\mathbf{x}, \theta)]^2 w(\mathbf{x}) d\mathbf{x} \quad (2)$$

where  $w(\cdot)$  is a known weighting function. According to Wong et al. (2017), the definition in Eq. (2) implies that the optimal calibration setting is *identifiable*, i.e., we can distinguish different calibration settings by evaluating the  $L_2$  distance between mean response surfaces of the physical system and the simulation model. Without loss of generality, we use equal weights  $w(\mathbf{x}) = 1$  in the rest of the paper.

We use a semiconductor production system as an example to illustrate simulation calibration. For a complex semiconductor production process involving thousands of steps, building an exact simulation model is almost impossible. In production scheduling, a class of simulation models based on a simplified queueing network is used to guide decision making (Horiguchi et al., 2001). Given a scheduling decision  $\mathbf{x}$ , we consider the expected cycle times  $\mu^p(\mathbf{x})$  of different types of products. Since the times staying at bottlenecks and near-bottlenecks dominate the cycle times, we model each bottleneck or near-bottleneck as a queueing station and aggregate the remaining stations. Given  $\mathbf{x}$ , the expected cycle time of simulation model  $\mu(\mathbf{x}, \theta)$  depends on the calibration setting  $\theta$ , i.e., parameters specifying the service distributions. To correctly guide the decision making for the real system, we first calibrate  $\theta$  to ensure that the expected cycle times estimated from the simulation system match with those of the real system. Then, the *calibrated* simulation system can be used to guide the scheduling decision.

However, the explicit forms of both  $\mu^p(\mathbf{x})$  and  $\mu(\mathbf{x}, \theta)$  are unknown in practice. The optimal calibration setting  $\theta^*$  can not be solved directly. Alternatively, we obtain the estimate of  $\theta^*$  by replacing the objective function in Eq. (2) with its expected value:

$$\hat{\theta}^* \in \operatorname{argmin}_{\theta \in \Theta} \int_{\mathcal{X}} E[\mu^p(\mathbf{x}) - \mu(\mathbf{x}, \theta)]^2 d\mathbf{x}, \quad (3)$$

where the expectation is taken with respect to the posterior distributions of  $\mu(\mathbf{x}, \theta)$  and  $\mu^p(\mathbf{x})$  given output data collected from the simulation model and the real system. The optimization problem in Eq. (3) can be solved empirically by using the data collected under different decisions and calibration settings. Since each simulation run could be computationally expensive, one-stage design is a luxury for large-scale simulation models, and a sequential data collection can be a feasible alternative. In this paper, we first consider a simplified situation that the decision is given at  $\mathbf{x}_0$ , and then we investigate how to navigate decision making along with simulation calibration. Through out this paper, we assume that the calibration parameter space  $\Theta$  contains a finite number of candidates, i.e.,

$$\Theta = \{\theta_1, \dots, \theta_M\}. \quad (4)$$

This assumption is adopted for simulation optimization and calibration in many studies; see for example Luo, Hong, Nelson, and Wu (2015) and Ryzhov (2018).

#### 3.1. Simplified simulation calibration

We first investigate the budget allocation issue among different calibration parameter settings. By simplifying the simulation calibration problem, we assume that the decision is fixed at a given point  $\mathbf{x}_0$ . This assumption is equivalent to the case that the simulation budget are evenly distributed over the decision space. Under a fixed decision policy, mean performances of the real system and the simulation model can be reduced to  $\mu^p$  and  $\mu(\theta)$ , respectively. Our objectives defining  $\theta^*$  and  $\hat{\theta}^*$  in Eqs. (2) and (3) are reduced to:

$$\theta^* \in \operatorname{argmin}_{\theta \in \Theta} [\mu^p - \mu(\theta)]^2 \quad \text{and} \quad \hat{\theta}^* \in \operatorname{argmin}_{\theta \in \Theta} E[\mu^p - \mu(\theta)]^2, \quad (5)$$

where the expectation is taken with regard to the posterior distributions of  $\mu^p$  and  $\mu(\theta)$ .

Following Ryzhov (2018), we assume that our current belief about  $\mu^p$  is characterized by a distribution with mean  $\hat{\mu}^p$  and standard deviation  $\sigma^p$ . Then, we write estimated optimal calibration setting Eq. (5) equivalently as,

$$\hat{\theta}^* \in \operatorname{argmin}_{\theta \in \Theta} E[\hat{\mu}^p - \mu(\theta)]^2. \quad (6)$$

Notice that  $E[\mu^p - \mu(\theta)]^2 = E[\hat{\mu}^p - \mu(\theta)]^2 + (\sigma^p)^2$ . Since  $\sigma^p$  does not impact the minimization over  $\theta \in \Theta$ , the expectation in Eq. (5) can be reduced to Eq. (6).

As noted earlier, it is more efficient to collect data in a sequential manner. In each step of the sequential procedure, we select a calibration setting to run simulations, and update our belief of  $\mu(\theta)$ , which further guides the acquisition of the calibration setting for the next simulation run. There are two key components in this procedure: (1) statistical model of  $\mu(\theta)$  for all  $\theta \in \Theta$ , and (2) a data collection policy to determine the calibration settings for new simulation runs. Section 4 discusses sequential data collection for simulation calibration under this simplified situation.

#### 3.2. Decision making with calibrated simulation model

To extend the calibration problem to the entire decision space, we return to the optimal calibration setting defined in Eq. (3). We assume that the information about  $\mu^p(\mathbf{x})$  is restricted to the observations at given design points  $\{\mathbf{x}_1, \dots, \mathbf{x}_K\}$ , and we are not able to obtain more physical data during the calibration and decision making procedure. Under this assumption, we approximate the optimal calibration setting by

$$\hat{\theta}^* \in \arg \min_{\theta \in \Theta} \sum_{k=1}^K E[\hat{\mu}^p(\mathbf{x}_k) - \mu(\mathbf{x}_k, \theta)]^2, \quad (7)$$

according to Wong et al. (2017). Similar to Eq. (6),  $\hat{\mu}^p(\mathbf{x}_k)$  is the mean of the posterior distribution of  $\mu^p(\mathbf{x}_k)$ , and the expectation in Eq. (7) is taken with respect to the posterior distribution of  $\mu(\mathbf{x}_k, \theta)$ . Notice that, we abuse the notation  $\hat{\theta}^*$  in both Eqs. (3) and (7). Once  $\hat{\theta}^*$  is determined, the optimal decision can be estimated by using the calibrated simulation model with the mean response  $\mu(\mathbf{x}, \hat{\theta}^*)$ :

$$\hat{\mathbf{x}}^* \in \arg \max_{\mathbf{x} \in \mathcal{X}} E[\mu(\mathbf{x}, \hat{\theta}^*)], \quad (8)$$

where the expectation is taken with regard to the posterior distribution of  $\mu(\mathbf{x}, \hat{\theta}^*)$ .

To sequentially collect data for both optimization and calibration, we consider three key components: (1) statistical model of  $\mu(\mathbf{x}, \theta)$ , (2) a data collection policy to determine the calibration setting of new simulation runs, and (3) a data collection policy to determine the decision point of new simulation runs in this paper.

#### 4. Simplified simulation calibration

This section follows the assumption in Section 3.1, i.e., simulation calibration with fixed decision point  $\mathbf{x}_0$ . We first review the sequential data collection procedure with summary statistics of simulation outputs. Then, a detailed sample path approach is proposed by modifying our early proposal in Wang et al. (2017).

##### 4.1. Simulation calibration via summary statistics

Under the calibration setting  $\theta$ , a simulation run generates one output sample path

$$\mathbf{Y}(\theta) = (Y_1(\theta), \dots, Y_L(\theta))^T, \quad (9)$$

where  $L$  is the fixed runlength. We assume that the outputs generated at warm-up stages have been taken off from this sample path. In the semiconductor production example mentioned above,  $Y_\ell(\theta)$  could be the cycle time of the  $\ell$ th order. Classical simulation approaches directly use the sample mean  $\bar{Y}(\theta) = \sum_{\ell=1}^L Y_\ell(\theta)/L$ . Suppose that it follows a normal distribution with mean  $\mu(\theta)$  and variance  $\lambda^2(\theta)$ . Under the finite calibration space assumption expressed in Eq. (4), we denote  $\mu_i \equiv \mu(\theta_i)$  and  $\lambda_i^2 \equiv \lambda^2(\theta_i)$  for  $i = 1, \dots, M$ , and assume that  $\mu_i$  and  $\lambda_i^2$  are independent across different calibration parameter settings. We use the normal-inverse-gamma distribution to surrogate our beliefs of  $\mu_i$  and  $\lambda_i^2$ ,

$$\mu_i | \lambda_i^2 \sim \mathcal{N}\left(\mu_i^{(0)}, \frac{\lambda_i^2}{\tau_i^{(0)}}\right), \quad \lambda_i^2 \sim \text{Inv}\Gamma(a_i^{(0)}, b_i^{(0)}). \quad (10)$$

For the sequential data collection procedure, a single simulation run is collected at each step. At the  $n$ th step, the chosen calibration setting is denoted by  $i^{(n)}$ , and the collected mean performance measure is denoted by  $\bar{Y}^{(n)} = \bar{Y}(\theta_{i^{(n)}})$ . The conjugacy property of the normal-inverse-gamma model updates the parameters at the  $i$ th calibration setting in Eq. (10). After the  $n$ th step, based on our current beliefs of the mean performances, the estimated optimal calibration setting in Eq. (5) can be expressed by

$$\hat{\theta}_s^*(n) = \arg \min_{\theta_i \in \Theta} \left\{ (\mu_i^{(n)} - \hat{\mu}^p)^2 + \sigma_i^{2,(n)} \right\}, \quad (11)$$

where  $\mu_i^{(n)}$  and  $\sigma_i^{2,(n)}$  are the posterior mean and variance of  $\mu_i$  at the  $n$ th step, and the sub-index  $s$  in  $\hat{\theta}_s^*(n)$  indicates the summary statistics approach. Ryzhov (2018) introduced the local time method

to select calibration parameter setting based on the belief about the mean performances at each step,

$$i^{(n)} = \arg \max_{\theta_i \in \Theta} l(i) \text{ with } l(i) = \sigma_i^{(n-1)} f\left(-\frac{|\mu_i^{(n-1)} - \hat{\mu}^p|}{\sigma_i^{(n-1)}}\right), \quad (12)$$

where  $f(z) = z\Phi(z) + \phi(z)$  with  $\phi$  and  $\Phi$  being the density and the cumulative distribution functions of the standard normal distribution.

By combining the Bayesian inference method for the mean performance and the local time criterion in Eq. (12), the optimal calibration parameter setting can be identified in a sequential manner. However, the summary statistics approach ignores the serial dependence of output sample paths, and potentially loses the accuracy in assessing the mean performances of candidate calibration settings, especially under a tight budget. By exploring the first two moments of dynamic behaviors carried in the simulation output sample paths, we propose a Bayesian sequential calibration approach in Section 4.2, and theoretically demonstrate its advantage over the classical summary statistics approach in Section 4.3.

##### 4.2. Simulation calibration via detailed sample paths

For any  $\theta \in \Theta$ , we assume that the sample path output  $\mathbf{Y}(\theta)$  in Eq. (9) follows a stationary Gaussian process with mean  $E[Y_\ell(\theta)] = \mu(\theta)$  for  $\ell = 1, \dots, L$ , and isotropic covariance  $\text{Cov}[Y_\ell(\theta), Y_{\ell'}(\theta)] = \sigma^2(\theta)r(|\ell - \ell'|; \theta)$  for  $\ell, \ell' = 1, \dots, L$ , where  $\sigma^2(\theta)$  denotes the variance, and  $r(\cdot; \theta)$  denotes the correlation function under the calibration parameter setting  $\theta$ . As an example, in the empirical study section, we consider the exponential correlation function, denoted by  $r(|\ell - \ell'|; \theta) = \rho_\theta^{|\ell - \ell'|}$ , where  $\rho_\theta$  denotes the correlation parameter depending on the calibration setting  $\theta$ . Even though the GP assumption does not hold in general, given a tight simulation budget, it provides a convenient way to model the first two moments of simulation outputs in a sample path.

Under the finite calibration space assumption in Eq. (4), the correlation matrix for sample path outputs with calibration setting  $\theta_i$  is denoted by  $R(\rho_i)$  for  $i = 1, \dots, M$ , where  $\rho_i$  is the correlation parameter. For simplification, we denote  $\mu_i \equiv \mu(\theta_i)$  and  $\sigma_i^2 \equiv \sigma^2(\theta_i)$ . The detailed simulation output  $\mathbf{Y}(\theta_i)$  is modeled as a realization from a multivariate normal distribution with a mean vector  $\mu_i \mathbf{1}_L$  and a covariance matrix  $\sigma_i^2 R(\rho_i)$ , where  $\mathbf{1}_L$  is an  $L$ -dimension vector with all entries loaded by one. We model our belief about  $\mu_i$  and  $\sigma_i^2$  by a normal-inverse-gamma conjugate prior

$$\mu_i | \sigma_i^2 \sim \mathcal{N}\left(\mu_i^{(0)}, \frac{\sigma_i^2}{q_i^{(0)}}\right), \quad \sigma_i^2 \sim \text{Inv}\Gamma(\alpha_i^{(0)}, \beta_i^{(0)}). \quad (13)$$

At the  $n$ th step, let  $i^{(n)}$  be the index of selected calibration setting for the next simulation run, and  $\mathbf{Y}^{(n)} = \mathbf{Y}(\theta_{i^{(n)}})$  be the newly collected sample path. The parameters in Eq. (13) will be updated as  $\mu_i^{(n)}$ ,  $q_i^{(n)}$ ,  $\alpha_i^{(n)}$  and  $\beta_i^{(n)}$ . Thus, the posterior mean of  $\mu_i$  is  $\mu_i^{(n)}$  as in Eq. (16) and the posterior variance of  $\mu_i$  can be derived as

$$\begin{aligned} \sigma_i^{2,(n)} &= \text{Var}(\mu_i) = \text{Var}[E(\mu_i | \sigma_i^2)] + E[\text{Var}(\mu_i | \sigma_i^2)] \\ &= \frac{\beta_i^{(n)}}{q_i^{(n)}(\alpha_i^{(n)} - 1)}, \end{aligned} \quad (14)$$

where the expectation and variance are taken with respect to the updated surrogate beliefs. Based on our beliefs of the mean performances at the  $n$ th step, the estimated optimal calibration setting in Eq. (5) can be expressed by

$$\hat{\theta}_d^*(n) = \arg \min_{\theta_i \in \Theta} \left\{ (\mu_i^{(n)} - \hat{\mu}^p)^2 + \sigma_i^{2,(n)} \right\}, \quad (15)$$

where the sub-index  $d$  in  $\hat{\theta}_d^*(n)$  represents the detailed sample path approach. According to the local time method in

Ryzhov (2018), we allocate new simulation runs by choosing the calibration setting that maximizes the local time criterion in Eq. (12) with the posterior mean and variance of  $\mu_i$  expressed in Eqs. (16) and (14).

Our conference paper (Wang et al., 2017) assumes that the correlation parameter  $\rho_i$  is known. Since an accurate estimate of  $\rho_i$  often requires a sufficient amount of simulation runs, it is not practical to assume that  $\rho_i$  can be accurately assessed, especially in early stage of the sequential procedure. In this paper, we update the empirical estimates of  $\hat{\rho}_i^{(n)}$  at each step by incorporating the available simulation outputs up to the  $n$ th step. By plugging the newly updated  $\hat{\rho}_i^{(n)}$  in the updating formulas of Proposition 1 in Wang et al. (2017), we obtain the the modified updating formulas:

$$\begin{aligned} \mu_i^{(n)} &= \mu_i^{(n-1)} + \frac{\mathbf{1}_L^\top R^{-1}(\hat{\rho}_i^{(n)})(\mathbf{Y}^{(n)} - \mu_i^{(n-1)}\mathbf{1}_L)}{q_i^{(n-1)} + \mathbf{1}_L^\top R^{-1}(\hat{\rho}_i^{(n)})\mathbf{1}_L}, \\ q_i^{(n)} &= q_i^{(n-1)} + \mathbf{1}_L^\top R^{-1}(\hat{\rho}_i^{(n)})\mathbf{1}_L, \quad \alpha_i^{(n)} = \alpha_i^{(n-1)} + \frac{L}{2}, \\ \beta_i^{(n)} &= \beta_i^{(n-1)} \\ &+ \frac{q_i^{(n-1)}(\mathbf{Y}^{(n)} - \mu_i^{(n-1)}\mathbf{1}_L)^\top R^{-1}(\hat{\rho}_i^{(n)})(\mathbf{Y}^{(n)} - \mu_i^{(n-1)}\mathbf{1}_L)}{2(q_i^{(n-1)} + \mathbf{1}_L^\top R^{-1}(\hat{\rho}_i^{(n)})\mathbf{1}_L)} \\ &+ \frac{\mathbf{1}_L^\top R^{-1}(\hat{\rho}_i^{(n)})(\mathbf{1}_L(\mathbf{Y}^{(n)})^\top - \mathbf{Y}^{(n)}\mathbf{1}_L^\top)R^{-1}(\hat{\rho}_i^{(n)})\mathbf{Y}^{(n)}}{2(q_i^{(n-1)} + \mathbf{1}_L^\top R^{-1}(\hat{\rho}_i^{(n)})\mathbf{1}_L)}, \end{aligned} \quad (16)$$

for  $i = i^{(n)}$ , whereas the parameters of the  $i$ th calibration setting maintain the same as the previous step for  $i \neq i^{(n)}$ .

We now discuss how to sequentially update the correlation parameters  $\hat{\rho}_i^{(n)}$  in Eq. (16). Given a choice of the correlation function  $r(\cdot; \theta)$ , the correlation parameters  $\hat{\rho}_i^{(n)}$  can be updated empirically by the maximum likelihood estimation approach (MLE). Since  $\mathbf{Y}_j$  can be viewed as a classical type of time-series response, the white likelihood approximation (Whittle, 1954) can be applied to obtain the MLE estimators efficiently.

For the exponential correlation function  $r(|\ell - \ell'|; \theta_i) = \rho_i^{|\ell - \ell'|}$ , a computational efficient implementation to approximate  $\hat{\rho}_i^{(n)}$  at each step can be developed to further simplify the Whittle likelihood approach. Proposition 1 gives the explicit expression to approximate the MLE estimator. The proof of Proposition 1 can be found in Appendix A.2. Under this approximation, the update formula in Eq. (16) is also computationally efficient. Notice that, the computational complexity of the inversion of the  $R(\hat{\rho}_i^{(n)})$  is  $O(L^3)$  with runlength  $L$ . However, under the proposed approximation with an exponential correlation function, the computational complexity of the inversion of correlation matrix is reduced to  $O(1)$ . For general correlation functions, by using the whittle approximation, the inversion of correlation matrix has the computational complexity  $O(L)$ . As a result of Proposition 1, the MLE estimator of the exponential correlation coefficient can be approximated by the sample lag-one correlation  $\hat{\rho}_i^{(n)}$  for large  $L$ ; say,  $L \geq 30$ , which holds in many situations.

**Proposition 1.** Let  $i = i^{(n)}$  be the calibration setting selected at the  $n$ th step. The sample paths obtained at  $\theta_i$  up to the current step are  $\{\mathbf{Y}^{(j)}(\theta_i)\}_{j=1}^{n_i}$ , where  $\mathbf{Y}^{(j)}(\theta_i) = (Y_1^{(j)}(\theta_i), \dots, Y_L^{(j)}(\theta_i))^\top$ . The MLE estimator of exponential correlation function parameter for the  $i$ th calibration setting is the solution of  $G(\rho_i) = (\rho_i c_2 - c_3)(1 - \rho_i^2) + L^{-1}(c_1 + \rho_i^2 c_2 - 2\rho_i c_3)\rho_i = 0$ , where  $c_1 = \sum_{j=1}^{n_i} \sum_{\ell=1}^{L-1} (Y_\ell^{(j)}(\theta_i) - \bar{y})^2$ ,  $c_2 = \sum_{j=1}^{n_i} \sum_{\ell=2}^{L-1} (Y_\ell^{(j)}(\theta_i) - \bar{y})^2$ ,  $c_3 = \sum_{j=1}^{n_i} \sum_{\ell=1}^{L-1} (Y_\ell^{(j)}(\theta_i) - \bar{y})(Y_{\ell+1}^{(j)}(\theta_i) - \bar{y})$ , and  $\bar{y} = \frac{1}{n_i L} \sum_{j=1}^{n_i} \sum_{\ell=1}^L Y_\ell^{(j)}(\theta_i)$ . As  $L$  is large, the MLE estimator can be

approximated with the sample lag-one correlation estimator:

$$\hat{\rho}_i^{(n)} = \frac{c_3}{c_2} = \frac{\sum_{j=1}^{n_i} \sum_{\ell=1}^{L-1} (Y_\ell^{(j)}(\theta_i) - \bar{y})(Y_{\ell+1}^{(j)}(\theta_i) - \bar{y})}{\sum_{j=1}^{n_i} \sum_{\ell=2}^{L-1} (Y_\ell^{(j)}(\theta_i) - \bar{y})^2},$$

which is an approximation of the solution to  $\tilde{G}(\rho_i) = (\rho_i c_2 - c_3)(1 - \rho_i^2) = G(\rho_i) + O_p(L^{-1}) = 0$ .

### 4.3. Asymptotic comparison

This section provides theoretical comparison between the summary statistics approach in Section 3 and the detailed sample path approach in Section 4.2. Our theories are developed based on the following conditions:

- (C1) The variances,  $\lambda_i^2$  in summary approach, and  $\sigma_i^2$  in detailed approach are known.
- (C2) The optimization problem in Eq. (5) has a unique optimal solution.
- (C3) The prior parameters in Eqs. (10) and (13) are non-informative, with mean equal to 0, and variance equal to  $\infty$ .

For different approaches, we evaluate the Expected Opportunity Cost (EOC):

$$EOC(\hat{\theta}^*) = E[(\mu(\hat{\theta}^*) - \mu^p)^2 - (\mu(\theta^*) - \mu^p)^2], \quad (17)$$

where  $\hat{\theta}^*$  is the estimated optimal calibration setting in Eq. (5) and  $\theta^*$  is the optimal calibration setting defined in Eq. (5). Since  $\theta^*$  attains the minimum of  $(\mu(\theta) - \mu^p)^2$ ,  $EOC(\hat{\theta}^*)$  is always non-negative. A smaller  $EOC(\hat{\theta}^*)$  indicates that  $\mu(\hat{\theta}^*)$  leads to a smaller distance between the means of the calibrated system and physical system. The advantage of the detailed sample path approach in terms of EOC can be shown in the following theorem, and the corresponding proof is provided in Appendix A.3.

**Theorem 2.** Under the conditions (C1)–(C3), for  $\hat{\theta}_d^*(n)$  in Eq. (15), and  $\hat{\theta}_s^*(n)$  in Eq. (11), we have that

$$EOC(\hat{\theta}_d^*(n)) \leq EOC(\hat{\theta}_s^*(n)),$$

if  $n$  is large enough.

Under the identifiable assumption in Eq. (2), it could be critical to evaluate the Probability of Correct Selection (PCS),

$$PCS(\hat{\theta}^*) = \Pr(\hat{\theta}^* = \theta^*). \quad (18)$$

According to Theorem 2 in our conference paper (Wang et al., 2017), we have shown that  $PCS(\hat{\theta}_d^*(n)) \geq PCS(\hat{\theta}_s^*(n))$ , if  $n$  is large enough. This result indicates that the calibration approach based detailed sample path has larger chance to identify the optimal calibration setting  $\theta^*$  than the approach based on the summary statistics.

## 5. Decision making with simulation calibration

This section extends the simplified calibration setting in Section 4 to calibrate simulation models for physical systems with a continuous decision space  $\mathcal{X}$ . As noted earlier, we only have observations from the physical system at the design points  $\{\mathbf{x}_1, \dots, \mathbf{x}_K\} \subset \mathcal{X}$ . The optimal calibration setting is defined by Eq. (7) accordingly. We propose a sequential data collection procedure for decision making along with simulation calibration. In Section 5.1, we introduce a Bayesian model with both decision parameter and calibration parameter. In Section 5.2, we develop a sequential data collection procedure so that we can simultaneously and efficiently calibrate the simulation model and guide decision making.

5.1. Bayesian models and parameter updating

For each calibration setting  $\theta$ , we surrogate the mean response surface of simulation model over the continuous decision space  $\mathcal{X}$  as a linear combination of basis functions:

$$\mu(\mathbf{x}, \theta) = \phi(\mathbf{x})^\top \mathbf{c}_\theta, \tag{19}$$

where  $\phi(\mathbf{x}) = (\phi(\mathbf{x}, \mathbf{x}_1), \dots, \phi(\mathbf{x}, \mathbf{x}_K))^\top$  is a vector of known basis functions, and knots of these basis functions are located at the design points  $\{\mathbf{x}_1, \dots, \mathbf{x}_K\}$  of the physical system, and  $\mathbf{c}_\theta = (c_1(\theta), \dots, c_K(\theta))^\top$  is a vector of coefficients with a multivariate normal prior. The model in Eq. (19) aggregates the information collected at discrete design points  $\{\mathbf{x}_1, \dots, \mathbf{x}_K\}$  to improve the prediction at any point of the continuous decision space  $\mathcal{X}$ . It has been proven to be effective in making prediction at decision points over  $\mathcal{X}$  (Cressie & Johannesson, 2008). As an example, the Gaussian basis function can be expressed by  $\phi(\mathbf{x}, \mathbf{x}_k) = \exp(-\sum_{i=1}^d t_i(x_i - x_{ki})^2)$ , where  $\mathbf{x} = (x_1, \dots, x_d)^\top \in \mathbb{R}^d$ , and  $t_i$ 's are the range parameters of these basis functions.

For a calibration setting  $\theta$  and a decision point  $\mathbf{x}$ , a simulation run generates a sample path,

$$\mathbf{Y}(\mathbf{x}, \theta) = (Y_1(\mathbf{x}, \theta), \dots, Y_L(\mathbf{x}, \theta))^\top, \tag{20}$$

where  $L$  is the runlength. For the summary statistic  $\bar{Y}(\mathbf{x}, \theta) = L^{-1} \sum_{\ell=1}^L Y_\ell(\mathbf{x}, \theta)$ , we assume that,

$$\bar{Y}(\mathbf{x}, \theta) = \mu(\mathbf{x}, \theta) + e_\theta, \tag{21}$$

where  $\mu(\mathbf{x}, \theta)$  is given by Eq. (19) and the simulation noise  $e_\theta \sim \mathcal{N}(0, \lambda_\theta^2)$ . At the  $n$ th step, our beliefs of mean response surface of the simulation model with different calibration settings are specified by

$$\mathbf{c}_\theta | \lambda_\theta^2 \sim \text{MVN}_K(\mathbf{c}_\theta^{(n)}, \lambda_\theta^2 (Q_\theta^{(n)})^{-1}), \quad \lambda_\theta^2 \sim \text{Inv}\Gamma(a_\theta^{(n)}, b_\theta^{(n)}), \tag{22}$$

where  $Q_\theta^{(n)}$  is a  $K \times K$  precision matrix. The prior parameters  $\mathbf{c}_\theta^{(n)}$ ,  $Q_\theta^{(n)}$ ,  $a_\theta^{(n)}$  and  $b_\theta^{(n)}$  can be updated according to Proposition 3.

**Proposition 3.** Given the Bayesian model Eqs. (19), (21) and (22), and the newly collected summary statistic  $\bar{Y}^{(n+1)} = \bar{Y}(\mathbf{x}^{(n+1)}, \theta^{(n+1)})$ , the parameters  $\mathbf{c}_\theta^{(n)}$ ,  $Q_\theta^{(n)}$ ,  $a_\theta^{(n)}$ , and  $b_\theta^{(n)}$  can be updated accordingly,

$$\begin{aligned} \mathbf{c}_\theta^{(n+1)} &= (Q_\theta^{(n+1)})^{-1} (Q_\theta^{(n)} \mathbf{c}_\theta^{(n)} + \bar{Y}^{(n+1)} \phi(\mathbf{x}^{(n+1)})), \\ Q_\theta^{(n+1)} &= Q_\theta^{(n)} + \phi(\mathbf{x}^{(n+1)}) \phi(\mathbf{x}^{(n+1)})^\top, \quad a_\theta^{(n+1)} = a_\theta^{(n)} + \frac{1}{2}, \\ b_\theta^{(n+1)} &= b_\theta^{(n)} + \frac{(\bar{Y}^{(n+1)} - \phi(\mathbf{x}^{(n+1)})^\top \mathbf{c}_\theta^{(n)})^2}{2(1 + \phi(\mathbf{x}^{(n+1)})^\top (Q_\theta^{(n)})^{-1} \phi(\mathbf{x}^{(n+1)}))}, \end{aligned} \tag{23}$$

for  $\theta = \theta^{(n+1)}$ , whereas the parameters of the other calibration setting remain the same as the previous step for  $\theta \neq \theta^{(n+1)}$ .

For a detailed sample path  $\mathbf{Y}(\mathbf{x}, \theta)$  in Eq. (20), we assume that

$$\mathbf{Y}(\mathbf{x}, \theta) = \mu(\mathbf{x}, \theta) \mathbf{1}_L + \boldsymbol{\varepsilon}_\theta, \tag{24}$$

where  $\boldsymbol{\varepsilon}_\theta$  is a zero mean GP with covariance function  $\text{Cov}[\varepsilon_\ell(\theta), \varepsilon_{\ell'}(\theta)] = \sigma^2(\theta) r(|\ell - \ell'|; \theta)$  and  $R_\theta = R(\rho_\theta)$  is the  $L \times L$  correlation matrix with the  $(\ell, \ell')$ th element equal to  $r(|\ell - \ell'|; \theta)$ . At the  $n$ th step, our beliefs of the mean response surface of simulation model with different calibration setting are modeled by,

$$\mathbf{c}_\theta | \sigma_\theta^2 \sim \text{MVN}_K(\mathbf{c}_\theta^{(n)}, \sigma_\theta^2 (Q_\theta^{(n)})^{-1}), \quad \sigma_\theta^2 \sim \text{Inv}\Gamma(\alpha_\theta^{(n)}, \beta_\theta^{(n)}). \tag{25}$$

The prior parameters  $\mathbf{c}_\theta^{(n)}$ ,  $Q_\theta^{(n)}$ ,  $\alpha_\theta^{(n)}$  and  $\beta_\theta^{(n)}$  can be updated according to Proposition 4.

**Proposition 4.** Given the Bayesian model Eqs. (19), (24) and (25), and the newly collected sample path  $\mathbf{Y}^{(n+1)} = \mathbf{Y}(\mathbf{x}^{(n+1)}, \theta^{(n+1)})$ , the parameters  $\mathbf{c}_\theta^{(n)}$ ,  $Q_\theta^{(n)}$ ,  $\alpha_\theta^{(n)}$ , and  $\beta_\theta^{(n)}$  can be updated as follows,

$$\begin{aligned} \mathbf{c}_\theta^{(n+1)} &= (Q_\theta^{(n+1)})^{-1} (Q_\theta^{(n)} \mathbf{c}_\theta^{(n)} + z_2^{(n+1)} \phi(\mathbf{x}^{(n+1)})), \\ Q_\theta^{(n+1)} &= Q_\theta^{(n)} + z_1 \phi(\mathbf{x}^{(n+1)}) \phi(\mathbf{x}^{(n+1)})^\top, \quad \alpha_\theta^{(n+1)} = \alpha_\theta^{(n)} + \frac{L}{2}, \\ \beta_\theta^{(n+1)} &= \beta_\theta^{(n)} \\ &+ \frac{1}{2} [z_3^{(n+1)} + (\mathbf{c}_\theta^{(n)})^\top Q_\theta^{(n)} \mathbf{c}_\theta^{(n)} - (\mathbf{c}_\theta^{(n+1)})^\top Q_\theta^{(n+1)} \mathbf{c}_\theta^{(n+1)}], \end{aligned} \tag{26}$$

for  $\theta = \theta^{(n+1)}$ , where

$$\begin{aligned} z_1 &= \mathbf{1}_L^\top R_\theta^{-1} \mathbf{1}_L, \quad z_2^{(n+1)} = \mathbf{1}_L^\top R_\theta^{-1} \mathbf{Y}^{(n+1)}, \quad \text{and} \\ z_3^{(n+1)} &= (\mathbf{Y}^{(n+1)})^\top R_\theta^{-1} \mathbf{Y}^{(n+1)}. \end{aligned}$$

The parameters of the calibration setting  $\theta \neq \theta^{(n+1)}$  remain the same as the previous step.

5.2. Sequential data collection policies

We propose sequential data collection policies to allocate design points for calibration and decision making at each step. At the  $n$ th step, a two-stage selection procedure is considered: (1) select calibration setting  $\theta^{(n+1)}$ , and (2) select decision setting  $\mathbf{x}^{(n+1)}$ . After determining  $\theta^{(n+1)}$  and  $\mathbf{x}^{(n+1)}$ , we collect the new simulation observation  $\bar{Y}^{(n+1)}$  (summary statistics) or  $\mathbf{Y}^{(n+1)}$  (detailed sample path) at  $(\theta^{(n+1)}, \mathbf{x}^{(n+1)})$ . The policies to select calibration setting and decision point are developed in this subsection.

For the design point of calibration parameter, we modify the local time method to accommodate multiple decision points:

$$\begin{aligned} i^{(n+1)} &= \arg \max_{\theta_i \in \Theta} \sum_{k=1}^K \ell(k, i) \quad \text{with } \ell(k, i) \\ &= \sigma_i^{(n)}(\mathbf{x}_k) f\left(-\frac{|\mu_i^{(n)}(\mathbf{x}_k) - \hat{\mu}^p(\mathbf{x}_k)|}{\sigma_i^{(n)}(\mathbf{x}_k)}\right), \end{aligned} \tag{27}$$

where

$$\sigma_i^{(n)}(\mathbf{x}_k) = \sqrt{\phi(\mathbf{x}_k)^\top (Q_\theta^{(n)})^{-1} \phi(\mathbf{x}_k) \frac{b_\theta^{(n)}}{a_\theta^{(n)} - 1}},$$

for the summary statistics, and

$$\sigma_i^{(n)}(\mathbf{x}_k) = \sqrt{\phi(\mathbf{x}_k)^\top (Q_\theta^{(n)})^{-1} \phi(\mathbf{x}_k) \frac{\beta_\theta^{(n)}}{\alpha_\theta^{(n)} - 1}}$$

for the detailed sample path, which can be derived similarly as Eq. (14). This policy aggregates local time criterion over the design points available for the physical system, and selects the most promising candidate in terms of approximating the physical observations.

Given the selected calibration setting at the  $(n + 1)$ th step as  $\theta^{(n+1)}$ , the decision can be made by

$$\max_{\mathbf{x} \in \mathcal{X}} \mu(\mathbf{x}, \theta^{(n+1)}), \tag{28}$$

which is an optimization problem with a blackbox objective. We solve this optimization problem under the Bayesian ranking and selection framework (Powell & Ryzhov, 2012). According to the surrogate model in Eq. (19), the knowledge gradient value (Qu, Ryzhov, Fu, & Ding, 2015) of the optimization problem in Eq. (28) can be expressed by

$$v^{(n+1)}(\mathbf{x}) = \mathbb{E}^n \left[ \max_{\mathbf{x}' \in \mathcal{X}} \phi(\mathbf{x}')^\top \mathbf{c}_\theta^{(n+1)} - \max_{\mathbf{x}'' \in \mathcal{X}} \phi(\mathbf{x}'')^\top \mathbf{c}_\theta^{(n)} \mid \mathbf{x}^{(n+1)} = \mathbf{x} \right],$$

$$= E^n \left[ \max_{\mathbf{x}' \in \mathcal{X}} \phi(\mathbf{x}')^\top \mathbf{c}_\theta^{(n+1)} \middle| \mathbf{x}^{(n+1)} = \mathbf{x} \right] - \max_{\mathbf{x}'' \in \mathcal{X}} \phi(\mathbf{x}'')^\top \mathbf{c}_\theta^{(n)}, \quad (29)$$

where the expectation  $E^n$  is taken with respect to the predictive distribution of  $\mathbf{c}_\theta^{(n+1)}$ , based on our beliefs before running the  $(n + 1)$ th simulation, and given that we select decision  $\mathbf{x}$  at the  $(n + 1)$ th step. Proposition 5 provides results to tackle those predictive distributions, and the proof of this proposition is deferred to Appendix A.6.

**Proposition 5.** Given the Bayesian model Eqs. (19), (21) and (22) for summary statistics or Eqs. (19), (24) and (25) for detailed sample path, the knowledge gradient value Eq. (29) can be expressed by,

$$v^{(n+1)}(\mathbf{x}) = E \left[ \max_{\mathbf{x}' \in \mathcal{X}} \mu^{(n)}(\mathbf{x}') + \tilde{s}^{(n)}(\mathbf{x}', \mathbf{x}) T_m \right] - \max_{\mathbf{x}'' \in \mathcal{X}} \mu^{(n)}(\mathbf{x}''), \quad (30)$$

where  $\mu^{(n)}(\mathbf{x}) = \phi(\mathbf{x})^\top \mathbf{c}_\theta^{(n)}$ , and

$$\tilde{s}^{(n)}(\mathbf{x}', \mathbf{x}) = \phi(\mathbf{x}')^\top (Q_\theta^{(n)})^{-1} \phi(\mathbf{x}) \sqrt{\frac{b_\theta^{(n)} [1 + \phi(\mathbf{x})^\top (Q_\theta^{(n)})^{-1} \phi(\mathbf{x})]}{a_\theta^{(n)}}},$$

for summary statistics,

$$\begin{aligned} \tilde{s}^{(n)}(\mathbf{x}', \mathbf{x}) &= \phi(\mathbf{x}')^\top (Q_\theta^{(n)})^{-1} \phi(\mathbf{x}) \sqrt{\frac{z_1 \beta_\theta^{(n)} [1 + z_1 \phi(\mathbf{x})^\top (Q_\theta^{(n)})^{-1} \phi(\mathbf{x})]}{\alpha_\theta^{(n)}}}, \end{aligned}$$

for detailed sample path approach, and  $T_m$  is a random variable following  $t$  distribution, with degree of freedom  $m = 2a_\theta^{(n)}$  for the summary statistics approach, and  $m = 2\alpha_\theta^{(n)}$  for the detailed sample path approach. The definition of  $z_1$  is the same as in Proposition 4.

According to Scott et al. (2011), we discretize  $\mathcal{X}$  in Eq. (30) to  $\{\mathbf{x}_1, \dots, \mathbf{x}_K, \mathbf{x}^{(1)}, \dots, \mathbf{x}^{(n)}\}$ ,

where  $\mathbf{x}_i$  with  $i = 1, \dots, K$  is the design point for physical system and  $\mathbf{x}^{(i)}$  with  $i = 1, \dots, n$  is the design point for the simulation model selected from the  $i$ th step. Then the expectation in Eq. (30) can be expressed explicitly via the same techniques in Section 5.3 of Powell and Ryzhov (2012). With the explicit expression of  $v^{(n+1)}(\mathbf{x})$ , we select  $\mathbf{x}^{(n+1)}$  by maximizing the knowledge gradient value  $\mathbf{x}^{(n+1)} = \operatorname{argmax}_{\mathbf{x} \in \mathcal{X}} v^{(n+1)}(\mathbf{x})$  as the decision point to be evaluated for the next simulation run. As a result, we select the calibration parameter setting and the decision point in a sequential manner to allocate simulation runs, and update our beliefs of expected response surfaces with different calibration settings. Once we have exhausted our simulation budget, the estimated optimal calibration setting and optimal decision is given by Eqs. (7) and (8), respectively. The entire procedure of sequential data collection for simulation calibration and decision making is summarized in Algorithm 1.

## 6. Empirical study

In this section, we provide numerical study to evaluate the finite sample behaviors and the robustness of our approaches. Section 6.1 compares the performance of the summary statistics calibration approach and the detailed sample path calibration approach under a fixed decision. Section 6.2 considers simulation calibration and decision making for a queueing network example.

### 6.1. Simplified simulation calibration

For the simplified simulation calibration, we compare the performance of three methods, including

---

**Algorithm 1:** Sequential data collection for decision making along with simulation calibration.

---

**Input:** Initial parameters  $\mathbf{c}_\theta^{(0)}$ ,  $Q_\theta^{(0)}$ ,  $a_\theta^{(0)}$ , and  $b_\theta^{(0)}$  for summary statistics (or  $\mathbf{c}_\theta^{(0)}$ ,  $Q_\theta^{(0)}$ ,  $\alpha_\theta^{(0)}$ , and  $\beta_\theta^{(0)}$  for detailed sample path), for each  $\theta_i$ ,  $i = 1, \dots, M$ .

**Output:** The estimated optimal calibration setting  $\hat{\theta}^*(n)$  and optimal decision  $\hat{\mathbf{x}}^*(n)$  at each step.

**for**  $n \leftarrow 1$  **to**  $N$  **do**

Choose calibration parameter setting  $\theta^{(n)}$  that maximizes aggregated local time criterion in Eq. (27);

For  $\theta^{(n)}$ , choose decision  $\mathbf{x}^{(n)}$  that maximizes the knowledge gradient value in Proposition 5;

Generate the simulation mean output  $\bar{Y}^{(n)}$  for summary statistics approach (sample path  $\mathbf{Y}^{(n)}$  for detailed sample path approach) at  $(\mathbf{x}^{(n)}, \theta^{(n)})$ ;

**for**  $i \leftarrow 1$  **to**  $M$  **do**

**if**  $\theta_i = \theta^{(n)}$  **then**

Update  $\mathbf{c}_{\theta_i}^{(n)}$ ,  $Q_{\theta_i}^{(n)}$ ,  $a_{\theta_i}^{(n)}$ , and  $b_{\theta_i}^{(n)}$  for summary statistics as in Proposition 3 (or  $\mathbf{c}_{\theta_i}^{(n)}$ ,  $Q_{\theta_i}^{(n)}$ ,  $\alpha_{\theta_i}^{(n)}$ , and  $\beta_{\theta_i}^{(n)}$  for detailed sample path as in Proposition 4).

**end**

**end**

Compute  $\hat{\theta}^*(n)$  as in Eq. (7);

Plug in  $\hat{\theta}^*(n)$  and compute  $\hat{\mathbf{x}}^*(n) = \max_{\mathbf{x} \in \mathcal{X}} \phi(\mathbf{x})^\top \mathbf{c}_{\hat{\theta}^*(n)}^{(n)}$

**end**

---

- **summary:** The summary statistics approach as described in Section 4.1.
- **detailed\_sw:** The proposed detailed sample path approach with stepwise estimation of correlation parameters as described in Section 4.2.
- **detailed\_kn:** The detailed sample path approach with known correlation matrix (Wang et al., 2017). In implementation, we use long-run steady-state simulation outputs to generate accurate correlation parameter estimates.

#### 6.1.1. Single server queues

We first consider  $M/M/1$  and  $M/G/1$  queues, which are the basic queueing models used in the simulation of manufacturing and service systems. The steady-state mean waiting time is the parameter of interests of these two examples.

**Example 6.1.1.  $M/M/1$  Queue:** We generate simulation output from an  $M/M/1$  queue with arrival rate 1, and the service rate is the calibration parameter. We consider seven cases with different values of mean performance in real system. The target mean response  $\mu^p$  is generated from an  $M/M/1$  queue with utilization equal to 0.3, 0.4, ..., 0.9, respectively. For each case, we consider  $M = 20$  calibration settings with the utilization of candidate systems equally spaced over  $[0.2, 0.95]$ . Each sample path has the warm-up equal to 200 and the runlength equal to  $L = 50$  in terms of number of finished customers.

**Example 6.1.2.  $M/G/1$  Queue:** We generate simulation output from  $M/G/1$  queue with arrival rate equal to 1. We consider six cases with the target mean response,  $\mu^p = 0.2, 0.5, 1, 1.5, 2, 3$ . For each case, there are  $M = 20$  candidate settings. The service times follow generalized Pareto distributions similar as the  $M/G/1$  example in Qu et al. (2015). We fix the shape parameter to be  $1/3$ , set location parameters as the calibration parameters  $\theta_i$  for  $i = 1, 2, \dots, 20$  equally spaced over  $[0.1, 0.65]$ , and scale parameters to be  $\theta_i/3$ .

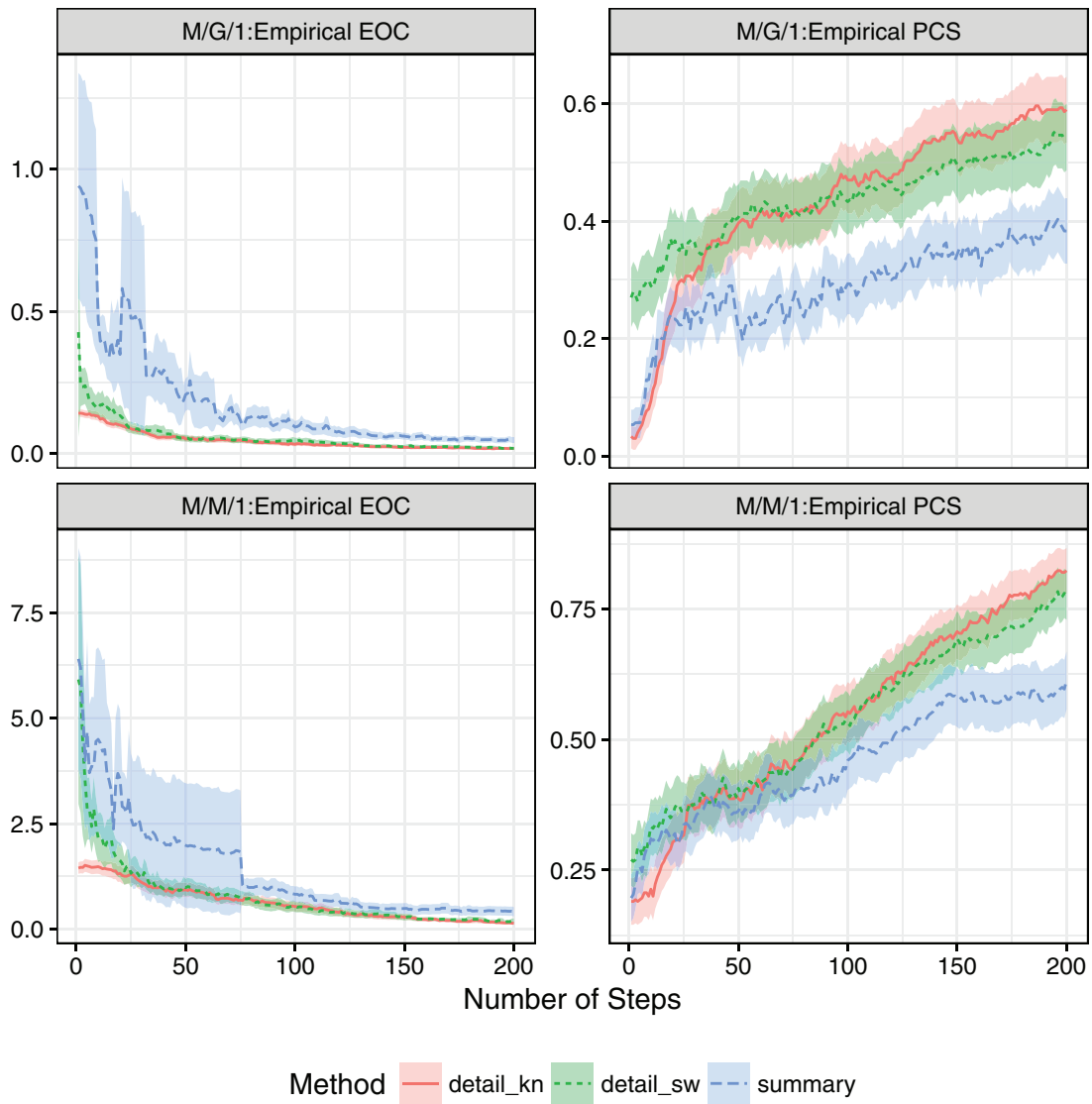


**Fig. 1.** Empirical EOC and PCS at each step of two examples from single service queue examples. Top panel:  $M/G/1$  example with target mean performance equal to 1; Bottom panel: the the  $M/M/1$  example with target utilization equal to 0.8. The figure shows that the “detailed\_sw” performs similar as “detailed\_kn” approach, and both outperforms “summary” approach.

Each sample path has the warm-up equal to 200 and the runlength equal to  $L = 50$ .

In all experiments, we compare the performance of the three approaches by using the empirical EOC and PCS estimated from 300 macro-replications (see Appendix A.7). All calibration procedures start with the same non-informative priors, and allocate five initial runs to each candidate calibration parameter setting. The top panel of Fig. 1 shows empirical EOC and PCS of  $M/G/1$  with target mean 1 and the bottom panel shows results for  $M/M/1$  with target utilization 0.8. The numerical results for different target utilization and mean performances are provided in Appendix A.8. We see that the detailed method with stepwise estimated correlation parameter (detail\_sw) acts similar as the detailed method with known correlation parameter (detail\_kn), and both outperform the summary statistics approach (summary). The error bars created by the 95% confidence intervals from the 300 replications show that both detail\_sw and detail\_kn are significantly better than the summary statistics approach for majority situations. As implied by Figs. A.10 and A.9, the performances of detail\_sw and detail\_kn are

significant better than that of the summary statistic approach over different values of the target mean  $\mu_p$ .

### 6.1.2. Jackson network example

Following Qu et al. (2015), we consider a classical 3-station open Jackson network as shown in the left panel of Fig. 2. Our goal is to accurately approximate the mean cycle time of the simulation system. The external arrivals follow a Poisson process with rate  $\lambda = 0.5$ , and the transition probabilities are also given in the left panel of Fig. 2. The service time at each station follows exponential distributions with rate  $\theta_1, \theta_2$  and  $\theta_3$ , respectively, where  $\theta_i \in [0.8, 2.2]$  for  $i = 1, 2, 3$ . A single sample path is generated with warm-up length equal to 1000 and runlength equal to  $L = 50$  in terms of finished entity. We generate  $M = 30$  candidate calibration parameter settings  $\theta_i = (\theta_{i1}, \theta_{i2}, \theta_{i3})$  for  $i = 1, 2, \dots, 30$  by using a maximin Latin-Hypercube design (Carnell, 2016) over the entire parameter space  $[0.8, 2.2]^3$ . The values of their mean cycle times are provided in the right panel of Fig. 2. Thus, we want to find the best combination of service rates at stations 1–3 among alternatives so that the mean cycle time of simulation model matches that of the

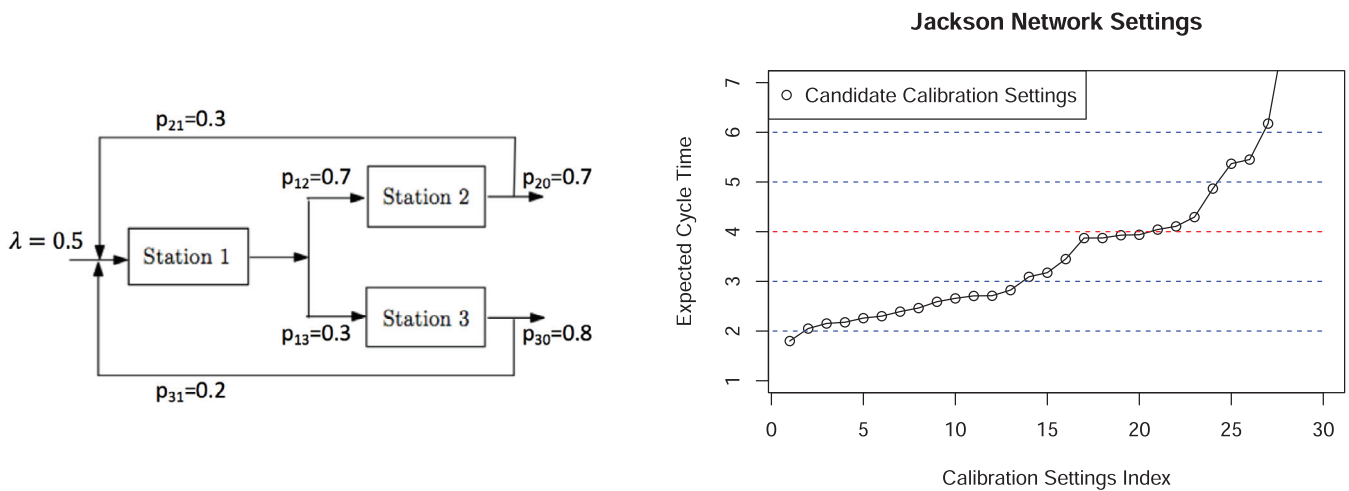


Fig. 2. Calibration settings of the 3-station Jackson network. Left panel: structure of the Jackson network; Right panel: the expected cycle time of calibration parameter settings generated from Latin-Hypercube design.

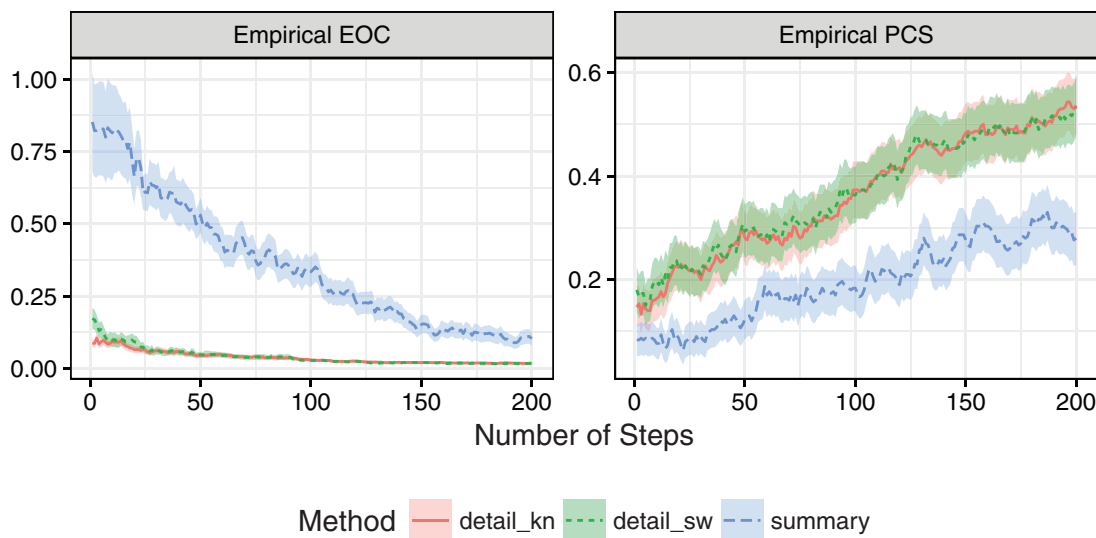


Fig. 3. Empirical EOC and PCS at each step of 3-station Jackson network examples with target mean performance equal to 3. The “detailed\_sw” performs similar as “detailed\_kn” approach, and both outperforms “summary” approach.

target real system. We consider five cases with  $\mu^p = 2, 3, 4, 5, 6$ , shown as the dashed horizontal lines in right panel of Fig. 2.

For the three alternative methods, we start with the same non-informative priors, and five initial runs are allocated to each candidate setting to build our original beliefs. For each level of target mean cycle time, the empirical EOC and PCS are estimated from 300 macro-replications. Fig. 3 provides results of the three approaches with the target mean cycle time  $\mu^p = 3$ . The numerical results under different levels of target mean  $\mu^p$  are summarized in Appendix A.8. This example gives similar observations as the simple Queueing models. As shown in the right panel of Fig. 2, several candidate settings (i.e., the circles with expected cycle times around four) have similar mean performance with  $\mu_p = 4$ . This situation belongs to the case that the optimal calibration setting can not be easily identified. Also as indicated in Fig. A.10, the PCS at  $\mu^p = 4$  (target mean) is lower than 30%, and the improvement is not significant by increasing the number of steps  $n$  from 50 to 500.

We now discuss our findings from the numerical results of the simplified simulation calibration. First, our numerical results validate the theoretical results in Section 4.3. The detailed sample path approaches (both “detailed\_sw” and “detailed\_kn”) outperform the

summary statistics approach in terms of EOC and PCS. By exploring the first two moments of serial outputs, the detailed sample path approaches are able to efficiently use the simulation resource and accurately assess the mean response with different calibration settings. Thus, it can improve the efficiency in simulation calibration, especially when the simulation budget is tight. Second, “detailed\_sw” and “detailed\_kn” have similar performances through these examples, which shows that the proposed stepwise correlation estimation approach in Proposition 1 is effective. Since the correlation parameter  $\rho$  in Eq. (16) can not be accurately estimated before the data collection procedure, the stepwise updated correlation parameter in “detailed\_sw” would be more practical for real applications. Third, the performance of our approach is robust to the GP assumption on the detailed output sample path even though it does not hold for some cases, e.g., queueing examples.

### 6.2. Decision making with simulation calibration for the Jackson network example

This section considers sequential data collection for simulation calibration along with decision making. We compare the detailed

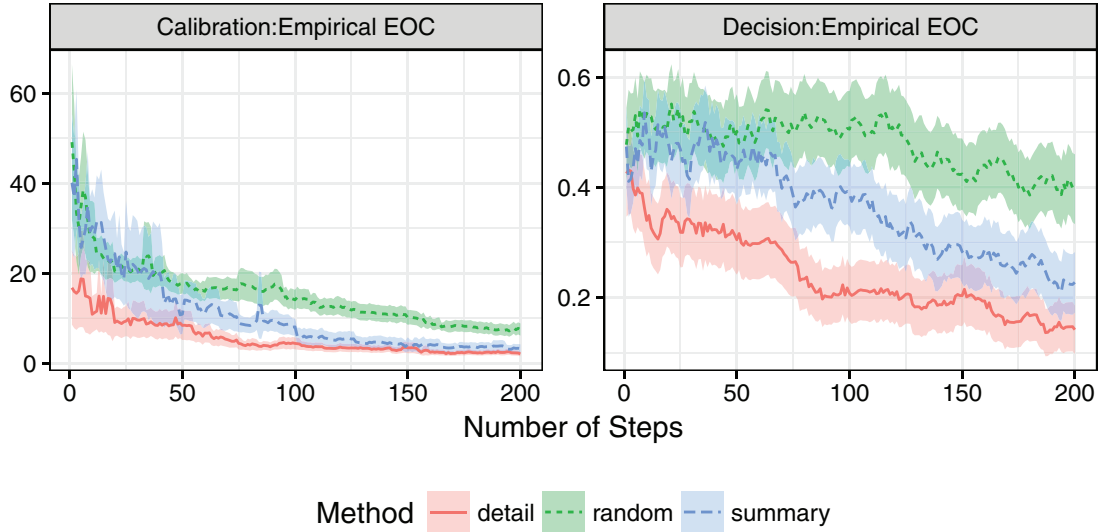


**Fig. 4.** Empirical EOC of calibration and decision with 95% confidence band at each step of the 3-station Jackson network for both calibration (left panel) and decision making (right panel). The figure shows detailed approach performs the best and random approach performs the worst among the three methods.

approach (“detail”) with summary statistics approach (“summary”) illustrated in Section 5. A naive alternative “random” is considered by replacing the data collection policies of the summary statistics approach with randomly selected candidate setting and decision in each iteration. We modify the Jackson Network example (Fig. 2) to study the decision making along with simulation calibration. Let the calibration parameter be the probability  $p_{12}$  in Fig. 2, which can be considered as the unknown product mix in production line. Let the decision  $x$  be the service rate at the first Station. Suppose that  $\theta \in \Theta \equiv \{0.75, 0.76, \dots, 0.85\}$  with eleven calibration settings evenly located between 0.75 and 0.85, and let  $\mathcal{X} = [0.8, 1.4]$ . The external arrivals follow a Poisson process with rate  $\lambda = 0.5$ . Let the service rates at Stations 2 and 3 be  $2 - x$  and 1, respectively. We set the true transition probabilities  $p_{12} = p_{20} = p_{30} = 0.8$ ,  $p_{13} = p_{21} = p_{31} = 0.2$ , which implies  $\theta^* = 0.8$ , and the warm-up equal to 1000 and the runlength equal to  $L = 50$  in terms of finished entities. Suppose we have observed data from physical system at  $K$  decision points evenly distributed on decision space  $\mathcal{X}$ . Our goal is to match the expected cycle time of simulation system with physical system and use the calibrated simulation to find the optimal decision  $x \in \mathcal{X}$  that minimizes this expected response.

For the three methods, we start with the same non-informative priors. Three initial runs are allocated at each candidate setting with decisions randomly chosen to form the prior distributions of the initial beliefs. Then we follow the sequential procedure proposed in Section 5. Fig. 4 gives results for  $K = 7$ . The left panel of Fig. 4 provides the empirical EOC for calibration that aggregated over observed decisions, the right panel shows the empirical EOC for decision:  $EOC(\hat{\mathbf{x}}^*) = E[\mu^p(\mathbf{x}^*) - \mu^p(\hat{\mathbf{x}}^*)]$ . The empirical EOCs for calibration and decision making are estimated from 200 macro-replications. Supplementary results for  $K = 5$  and 10 are given in Appendix A.8. The results show that the detailed approach is significantly better than both random and summary statistics approach in terms of calibration (left panel in Fig. 4) and decision making (right panel in Fig. 4).

### 7. Conclusions

In this paper, we develop the mean performance calibration approach for the situations where each simulation run is computationally expensive and the simulation budget is tight. Build on the knowledge of sample path time series information, we propose a

new Bayesian sequential data collection method for calibrating system mean performance. The proposed method can efficiently make use of the simulation resources to allocate more simulation runs to the promising candidates and improve the calibration accuracy. We further develop a sequential framework that incorporates decision making along with calibration. It improves decision making with the calibrated simulation model. Numerical and theoretical results show the effectiveness of our proposal.

We remark on the directions for future research as following. First, we can further incorporate correlation between calibration parameter settings, or extend the current calibration to the continuous calibration parameter space. Second, instead of the fixed target  $\hat{\mu}^p$  or  $\hat{\mu}^p(\mathbf{x})$ , the proposed work could be generalized to consider performance measure estimated and also dynamically updated by using data sequentially collected from the real system.

### Appendix A

#### A1. Inverse of exponential correlation matrix

For the exponential correlation case  $\text{Corr}[Y_{\ell}(\boldsymbol{\theta}_i), Y_{\ell'}(\boldsymbol{\theta}_i)] = r(|\ell - \ell'|; \boldsymbol{\theta}_i) = \rho_i^{|\ell - \ell'|}$ , the inverse of correlation matrix is,

$$R^{-1}(\rho_i) = \frac{1}{1 - \rho_i^2} \begin{bmatrix} 1 & -\rho_i & 0 & \dots & 0 & 0 \\ -\rho_i & 1 + \rho_i^2 & -\rho_i & \dots & 0 & 0 \\ \dots & \dots & \dots & \dots & \dots & \dots \\ 0 & 0 & 0 & \dots & 1 + \rho_i^2 & -\rho_i \\ 0 & 0 & 0 & \dots & -\rho_i & 1 \end{bmatrix}. \tag{A.1}$$

#### A2. Proof of Proposition 1

Notice that  $\mathbf{Y}^{(j)}(\boldsymbol{\theta}_i) = (Y_1^{(j)}(\boldsymbol{\theta}_i), \dots, Y_L^{(j)}(\boldsymbol{\theta}_i))^T \sim \mathcal{MVN}_L(\mu_i \mathbf{1}_L, \sigma_i^2 R(\rho_i))$ , we have the likelihood,

$$\begin{aligned} & p(\mu_i, \sigma_i^2, \rho_i; \{\mathbf{Y}^{(j)}(\boldsymbol{\theta}_i)\}_{j=1}^{n_i}) \\ & \propto (\sigma_i^2)^{-\frac{n_i L}{2}} (1 - \rho_i^2)^{-\frac{n_i(L-1)}{2}} \\ & \cdot \exp \left[ -\frac{1}{2\sigma_i^2} \sum_{j=1}^{n_i} (\mathbf{Y}^{(j)}(\boldsymbol{\theta}_i) - \mu_i \mathbf{1}_L)^T R^{-1}(\rho_i) (\mathbf{Y}^{(j)}(\boldsymbol{\theta}_i) - \mu_i \mathbf{1}_L) \right], \end{aligned}$$

and the log-likelihood,

$$\begin{aligned} & \log p(\mu_i, \sigma_i^2, \rho_i; \{\mathbf{Y}^{(j)}(\boldsymbol{\theta}_i)\}_{j=1}^{n_i}) \\ & \propto -\frac{n_i L}{2} \log(\sigma_i^2) - \frac{n_i(L-1)}{2} \log(1 - \rho_i^2) \\ & \quad - \frac{1}{2\sigma_i^2} \sum_{j=1}^{n_i} (\mathbf{Y}^{(j)}(\boldsymbol{\theta}_i) - \mu_i \mathbf{1}_L)^\top R^{-1}(\rho_i) (\mathbf{Y}^{(j)}(\boldsymbol{\theta}_i) - \mu_i \mathbf{1}_L). \end{aligned}$$

Take derivative with respect to  $\mu_i$  and set to be zero,

$$\frac{1}{\sigma_i^2} \mathbf{1}_L^\top R^{-1}(\rho_i) \left( \mu_i - \frac{1}{n} \sum_{j=1}^{n_i} \mathbf{Y}^{(j)}(\boldsymbol{\theta}_i) \right) = 0.$$

We plug in the inverse of correlation matrix provided by Appendix A.1 and solve for  $\mu_i$ . Then the maximum likelihood estimator for  $\mu_i$  can be approximate by sample mean for large enough  $L$ ,

$$\hat{\mu}_i = \frac{\mathbf{1}_L^\top R^{-1}(\rho_i) \bar{\mathbf{Y}}}{\mathbf{1}_L^\top R^{-1}(\rho_i) \mathbf{1}_L} = \frac{\sum_{\ell=1}^L \bar{Y}_\ell - \rho_i \sum_{\ell=2}^{L-1} \bar{Y}_\ell}{L - \rho_i(L-2)} \rightarrow \bar{y}, \quad (\text{as } L \rightarrow \infty)$$

where

$$\bar{\mathbf{Y}} = \frac{1}{n_i} \sum_{j=1}^{n_i} \mathbf{Y}^{(j)}(\boldsymbol{\theta}_i) = (\bar{Y}_1, \bar{Y}_2, \dots, \bar{Y}_L), \quad \text{and}$$

$$\bar{y} = \frac{1}{n_i L} \sum_{j=1}^{n_i} \sum_{\ell=1}^L Y_\ell^{(j)}(\boldsymbol{\theta}_i).$$

Further, we can obtain the MLE for  $\sigma_i^2$  by plug in the  $\hat{\mu}_i$ ,

$$\hat{\sigma}_i^2 = \frac{1}{n_i L} \sum_{j=1}^{n_i} (\mathbf{Y}^{(j)}(\boldsymbol{\theta}_i) - \bar{y} \mathbf{1}_L)^\top R^{-1}(\rho_i) (\mathbf{Y}^{(j)}(\boldsymbol{\theta}_i) - \bar{y} \mathbf{1}_L).$$

After that, by plugging  $\hat{\mu}_i$  and  $\hat{\sigma}_i^2$  in the negative log likelihood,

$$\begin{aligned} & -\log p(\hat{\mu}_i, \hat{\sigma}_i^2, \rho_i) \\ & \propto \frac{n_i L}{2} \log \left[ \sum_{j=1}^{n_i} (\mathbf{Y}^{(j)}(\boldsymbol{\theta}_i) - \bar{y} \mathbf{1}_L)^\top R^{-1}(\rho_i) (\mathbf{Y}^{(j)}(\boldsymbol{\theta}_i) - \bar{y} \mathbf{1}_L) \right] \\ & \quad + \frac{n_i(L-1)}{2} \log(1 - \rho_i^2) \\ & \propto \frac{n_i L}{2} \log \left[ \frac{c_1 + \rho_i^2 c_2 - 2\rho_i c_3}{1 - \rho_i^2} \right] + \frac{n_i(L-1)}{2} \log(1 - \rho_i^2) \\ & \propto \log \frac{[c_1 + \rho_i^2 c_2 - 2\rho_i c_3]^L}{1 - \rho_i^2}. \end{aligned}$$

where  $c_1 = \sum_{j=1}^{n_i} \sum_{\ell=1}^L (Y_\ell^{(j)}(\boldsymbol{\theta}_i) - \bar{y})^2$ ,  $c_2 = \sum_{j=1}^{n_i} \sum_{\ell=2}^{L-1} (Y_\ell^{(j)}(\boldsymbol{\theta}_i) - \bar{y})^2$ ,  $c_3 = \sum_{j=1}^{n_i} \sum_{\ell=1}^{L-1} (Y_\ell^{(j)}(\boldsymbol{\theta}_i) - \bar{y})(Y_{\ell+1}^{(j)}(\boldsymbol{\theta}_i) - \bar{y})$ . To solve the MLE for  $\rho_i$ , set the partial-derivative with respect to  $\rho_i$  to be 0,

$$L(\rho_i c_2 - c_3)(1 - \rho_i^2) + (c_1 + \rho_i^2 c_2 - 2\rho_i c_3)\rho_i = 0,$$

so as  $L$  being large enough,

$$\hat{\rho}_i \rightarrow \frac{c_3}{c_2} = \frac{\sum_{j=1}^{n_i} \sum_{\ell=1}^{L-1} (Y_\ell^{(j)}(\boldsymbol{\theta}_i) - \bar{y})(Y_{\ell+1}^{(j)}(\boldsymbol{\theta}_i) - \bar{y})}{\sum_{j=1}^{n_i} \sum_{\ell=2}^{L-1} (Y_\ell^{(j)}(\boldsymbol{\theta}_i) - \bar{y})^2} \quad (\text{as } L \rightarrow \infty)$$

### A3. Proof of Theorem 2

The expected opportunity cost, under assumptions (C1)–(C3) and  $\mu^p = 0 < \mu_1 < \mu_2 < \dots < \mu_M$ , can be reduced to,

$$\text{EOC}(\hat{\boldsymbol{\theta}}^*) = E[\mu(\hat{\boldsymbol{\theta}}^*)^2] - \mu_2^2$$

For convenience, we denote  $\hat{\mu}^{(m)} = \mu(\hat{\boldsymbol{\theta}}_m^*(n))$ , where  $m = d, s$ , indicating the calibration method, and,

$$p_i^{(m)} = \Pr(\hat{\mu}^{(m)} = \mu_i \mid \hat{\mu}^{(m)} > \mu_{i-1}), \quad \text{for } i = 2, \dots, M-1,$$

$$p_1^{(m)} = \Pr(\hat{\mu}^{(m)} = \mu_1)$$

$$q_i^{(m)} = 1 - p_i^{(m)}, \quad \text{for } i = 1, \dots, M-1$$

$$\zeta_i^{(m)} = E[\hat{\mu}^{(m)2} \mid \hat{\mu}^{(m)} > \mu_i], \quad \text{for } i = 1, \dots, M-1,$$

$$\zeta_0^{(m)} = E[\hat{\mu}^{(m)2}],$$

where  $\hat{\mu}^{(m)2}$  denotes the square of  $\hat{\mu}^{(m)}$ . We want to show that  $\zeta_0^{(d)} \leq \zeta_0^{(s)}$ , since

$$\zeta_{i-1}^{(m)} = \mu_i^2 p_i^{(m)} + \zeta_i^{(m)} q_i^{(m)},$$

and  $\zeta_{M-1}^{(m)} = E[\hat{\mu}^{(m)2} \mid \hat{\mu}^{(m)} > \mu_{M-1}] = \mu_M^2$ . It is straightforward to show

$$\begin{aligned} \zeta_0^{(m)} &= \mu_1^2 p_1^{(m)} + \mu_2^2 p_2^{(m)} q_1^{(m)} + \dots + \mu_{M-1}^2 p_{M-1}^{(m)} q_1^{(m)} q_2^{(m)} \dots q_{M-2}^{(m)} \\ & \quad + \mu_M^2 q_1^{(m)} q_2^{(m)} \dots q_{M-1}^{(m)} \\ &= \mu_1^2 + \sum_{i=1}^{M-1} (\mu_{i+1}^2 - \mu_i^2) \prod_{j=1}^i q_j^{(m)} \end{aligned} \quad (\text{A.2})$$

Notice that  $p_1^{(m)}$  is exactly the PCS of each method, and  $p_i^{(m)}$  is the PCS of calibration that ignoring first  $(i-1)$  alternatives (for  $i = 2, \dots, M-1$ ). Following the similar procedure proving Theorem 2 in Wang et al. (2017),

$$\text{PCS}(\hat{\boldsymbol{\theta}}_d^*(n)) \geq \text{PCS}(\hat{\boldsymbol{\theta}}_s^*(n)),$$

we can analogously show  $p_i^{(d)} \geq p_i^{(s)}$  or equivalently  $q_i^{(d)} \leq q_i^{(s)}$ . Thus, we have  $\zeta_0^{(d)} \leq \zeta_0^{(s)}$ , and further,

$$\text{EOC}(\hat{\boldsymbol{\theta}}_d^*(n)) \leq \text{EOC}(\hat{\boldsymbol{\theta}}_s^*(n))$$

### A4. Proof of Proposition 3

For summary statistics (mean response) from the stochastic simulation, the data model and surrogate beliefs are provided by Eqs. (19), (21) and (22). Suppose at the  $n+1$ th step, we select calibration parameter setting  $\boldsymbol{\theta}^{(n+1)} = \boldsymbol{\theta}$  and decision  $\mathbf{x}^{(n+1)} = \mathbf{x}$  to run simulation and obtain  $\bar{Y}^{(n+1)} = \bar{Y}(\mathbf{x}, \boldsymbol{\theta})$ , then we have,

$$\bar{Y}^{(n+1)} \sim \mathcal{N}(\boldsymbol{\phi}(\mathbf{x})^\top \mathbf{c}_\theta, \lambda_\theta^2),$$

and the prior of hyperparameters  $\mathbf{c}_\theta$  and  $\lambda_\theta^2$  are given through Eq. (22), so we can compute the posterior,

$$\begin{aligned} & p(\mathbf{c}_\theta, \lambda_\theta^2 \mid \bar{Y}^{(n+1)}) \\ & \propto (\lambda_\theta^2)^{-a_\theta^{(n)} - (K+3)/2} \exp \left\{ -\frac{1}{2\lambda_\theta^2} (\bar{Y}^{(n+1)} - \boldsymbol{\phi}(\mathbf{x})^\top \mathbf{c}_\theta)^2 \right\} \\ & \quad \cdot \exp \left\{ -\frac{1}{2\lambda_\theta^2} (\mathbf{c}_\theta - \mathbf{c}_\theta^{(n)})^\top Q_\theta^{(n)} (\mathbf{c}_\theta - \mathbf{c}_\theta^{(n)}) \right\} \cdot \exp \left\{ -\frac{b_\theta^{(n)}}{\lambda_\theta^2} \right\} \\ & \propto (\lambda_\theta^2)^{-a_\theta^{(n)} - (K+3)/2} \\ & \quad \cdot \exp \left\{ -\frac{1}{2\lambda_\theta^2} (\mathbf{c}_\theta - \mathbf{c}_\theta^{(n+1)})^\top Q_\theta^{(n+1)} (\mathbf{c}_\theta - \mathbf{c}_\theta^{(n+1)}) \right\} \\ & \quad \cdot \exp \left\{ -\frac{b_\theta^{(n)}}{\lambda_\theta^2} - \frac{1}{2\lambda_\theta^2} [\bar{Y}^{(n+1),2} + (\mathbf{c}_\theta^{(n)})^\top Q_\theta^{(n)} \mathbf{c}_\theta^{(n)} \right. \\ & \quad \left. - (\mathbf{c}_\theta^{(n+1)})^\top Q_\theta^{(n+1)} \mathbf{c}_\theta^{(n+1)}] \right\} \end{aligned}$$

$$\begin{aligned} &\propto (\lambda_\theta^2)^{-K} \\ &\times \exp \left\{ -\frac{1}{2\lambda_\theta^2} (\mathbf{c}_\theta - \mathbf{c}_\theta^{(n+1)})^\top Q_\theta^{(n+1)} (\mathbf{c}_\theta - \mathbf{c}_\theta^{(n+1)}) \right\} \\ &\cdot (\lambda_\theta^2)^{-a_\theta^{(n+1)}-1} \exp \left\{ -\frac{b_\theta^{(n+1)}}{\lambda_\theta^2} \right\}, \end{aligned}$$

still follows multivariate-normal-inverse-gamma distribution, where  $\mathbf{c}_\theta^{(n+1)}$ ,  $Q_\theta^{(n+1)}$ ,  $a_\theta^{(n+1)}$ , and  $b_\theta^{(n+1)}$  are given by Eq. (23). Notice the updating formula for  $b_\theta^{(n+1)}$  is obtained by plugging in  $\mathbf{c}_\theta^{(n+1)}$ ,  $Q_\theta^{(n+1)}$ , and applying Sherman–Morrison formula on inverse of  $Q_\theta^{(n+1)}$ .

A5. Proof of Proposition 4

Similarly, for detailed sample path from the stochastic simulation, the data model and surrogate beliefs are provided by Eqs. (19), (24) and (25). Suppose at the  $n + 1$ th step, we select calibration parameter setting  $\theta^{(n+1)} = \theta$  and decision  $\mathbf{x}^{(n+1)} = \mathbf{x}$  to run simulation and obtain  $\mathbf{Y}^{(n+1)} = \mathbf{Y}(\mathbf{x}, \theta)$ , then we have,

$$\mathbf{Y}^{(n+1)} \sim \mathcal{M}\mathcal{V}\mathcal{N}_L(\phi(\mathbf{x})^\top \mathbf{c}_\theta \mathbf{1}_L, \sigma_\theta^2 R_\theta),$$

and the prior of hyperparameters  $\mathbf{c}_\theta$  and  $\lambda_\theta^2$  are given through Eq. (25), so we can compute the posterior,

$$\begin{aligned} p(\mathbf{c}_\theta, \sigma_\theta^2 | \mathbf{Y}^{(n+1)}) &\propto (\sigma_\theta^2)^{-\alpha_\theta^{(n)} - (K+L)/2-1} \\ &\cdot \exp \left\{ -\frac{1}{2\sigma_\theta^2} (\mathbf{Y}^{(n+1)} - \phi(\mathbf{x})^\top \mathbf{c}_\theta \mathbf{1}_L)^\top R_\theta^{-1} (\mathbf{Y}^{(n+1)} - \phi(\mathbf{x})^\top \mathbf{c}_\theta \mathbf{1}_L) \right\} \\ &\cdot \exp \left\{ -\frac{1}{2\sigma_\theta^2} (\mathbf{c}_\theta - \mathbf{c}_\theta^{(n)})^\top Q_\theta^{(n)} (\mathbf{c}_\theta - \mathbf{c}_\theta^{(n)}) \right\} \cdot \exp \left\{ -\frac{\beta_\theta^{(n)}}{\sigma_\theta^2} \right\} \\ &\propto (\sigma_\theta^2)^{-\alpha_\theta^{(n)} - (K+L)/2-1} \\ &\times \exp \left\{ -\frac{1}{2\sigma_\theta^2} (\mathbf{c}_\theta - \mathbf{c}_\theta^{(n+1)})^\top Q_\theta^{(n+1)} (\mathbf{c}_\theta - \mathbf{c}_\theta^{(n+1)}) \right\} \\ &\cdot \exp \left\{ -\frac{\beta_\theta^{(n)}}{\sigma_\theta^2} - \frac{1}{2\sigma_\theta^2} [z_3 + (\mathbf{c}_\theta^{(n)})^\top Q_\theta^{(n)} \mathbf{c}_\theta^{(n)} \right. \\ &\quad \left. - (\mathbf{c}_\theta^{(n+1)})^\top Q_\theta^{(n+1)} \mathbf{c}_\theta^{(n+1)}] \right\} \\ &\propto (\sigma_\theta^2)^{-K} \exp \left\{ -\frac{1}{2\sigma_\theta^2} (\mathbf{c}_\theta - \mathbf{c}_\theta^{(n+1)})^\top Q_\theta^{(n+1)} (\mathbf{c}_\theta - \mathbf{c}_\theta^{(n+1)}) \right\} \\ &\cdot (\lambda_\theta^2)^{-\alpha_\theta^{(n+1)}-1} \exp \left\{ -\frac{\beta_\theta^{(n+1)}}{\lambda_\theta^2} \right\}, \end{aligned}$$

still follows multivariate-normal-inverse-gamma distribution, where  $\mathbf{c}_\theta^{(n+1)}$ ,  $Q_\theta^{(n+1)}$ ,  $a_\theta^{(n+1)}$ ,  $b_\theta^{(n+1)}$  are given by Eq. (26).

A6. Proof of Proposition 5

**Predictive distribution for summary statistics:** According to Eqs. (21) and (22) and given  $\mathbf{x}^{(n+1)} = \mathbf{x}$ , we can easily see,

$$\bar{Y}^{(n+1)} | \lambda_\theta^2 \sim \mathcal{N}(\phi(\mathbf{x})^\top \mathbf{c}_\theta^{(n)}, \lambda_\theta^2 [1 + \phi(\mathbf{x})^\top (Q_\theta^{(n)})^{-1} \phi(\mathbf{x})]),$$

so that  $\bar{Y}^{(n+1)}$  and  $\lambda_\theta^2$  together follow a normal-inverse-gamma, the predictive distribution of  $\bar{Y}^{(n+1)}$  is a t-distribution,

$$\bar{Y}^{(n+1)} = \phi(\mathbf{x})^\top \mathbf{c}_\theta^{(n)} + \sqrt{\frac{b_\theta^{(n)} [1 + \phi(\mathbf{x})^\top (Q_\theta^{(n)})^{-1} \phi(\mathbf{x})]}{a_\theta^{(n)}}} \cdot T_{2a_\theta^{(n)}},$$

where  $T_{2a_\theta^{(n)}}$  is a standard t-distributed random variable with degree of freedom  $2a_\theta^{(n)}$ . Then, by Eq. (23), the predictive distribution of  $\phi(\mathbf{x}')^\top \mathbf{c}_\theta^{(n+1)}$ ,

$$\begin{aligned} \phi(\mathbf{x}')^\top \mathbf{c}_\theta^{(n+1)} &= \phi(\mathbf{x}')^\top \mathbf{c}_\theta^{(n)} \\ &\quad + \phi(\mathbf{x}')^\top (Q_\theta^{(n)})^{-1} \phi(\mathbf{x}) \\ &\quad \times \sqrt{\frac{b_\theta^{(n)} [1 + \phi(\mathbf{x})^\top (Q_\theta^{(n)})^{-1} \phi(\mathbf{x})]}{a_\theta^{(n)}}} \cdot T_{2a_\theta^{(n)}}. \end{aligned} \tag{A.3}$$

**Predictive distribution for detailed sample path:** Similarly, by Eqs. (24) and (25), we can see  $\mathbf{Y}^{(n+1)}$  and  $\sigma_\theta^2$  follow multivariate-normal-inverse-gamma, so that  $z_2^{(n+1)} = \mathbf{1}_L^\top R_\theta^{-1} \mathbf{Y}^{(n+1)}$  and  $\sigma_\theta^2$  follow normal-inverse-gamma. Given  $\mathbf{x}^{(n+1)} = \mathbf{x}$ , the predictive distribution of  $z_2^{(n+1)}$ ,

$$\begin{aligned} z_2^{(n+1)} &= z_1 \phi(\mathbf{x})^\top \mathbf{c}_\theta^{(n)} \\ &\quad + \sqrt{\frac{z_1 \beta_\theta^{(n)} [1 + z_1 \phi(\mathbf{x})^\top (Q_\theta^{(n)})^{-1} \phi(\mathbf{x})]}{\alpha_\theta^{(n)}}} \cdot T_{2\alpha_\theta^{(n)}}, \end{aligned}$$

and the predictive distribution of  $\phi(\mathbf{x}')^\top \mathbf{c}_\theta^{(n+1)}$  can be derived from Eq. (26),

$$\begin{aligned} \phi(\mathbf{x}')^\top \mathbf{c}_\theta^{(n+1)} &= \phi(\mathbf{x}')^\top \mathbf{c}_\theta^{(n)} + \phi(\mathbf{x}')^\top (Q_\theta^{(n)})^{-1} \phi(\mathbf{x}) \\ &\quad \times \sqrt{\frac{z_1 \beta_\theta^{(n)} [1 + z_1 \phi(\mathbf{x})^\top (Q_\theta^{(n)})^{-1} \phi(\mathbf{x})]}{\alpha_\theta^{(n)}}} \cdot T_{2\alpha_\theta^{(n)}}. \end{aligned} \tag{A.4}$$

Then the Proposition 5 follows naturally.

A7. Empirical measurement of calibration

Here we explicitly provide the notations and expressions of the empirical criterion (i.e., EOC and PCS) that we used in Section 6. The empirical EOC is calculated as the average opportunity cost over macro-replications,

$$\widehat{\text{EOC}} = \frac{1}{B} \sum_{b=1}^B [(\mu(\hat{\theta}^{(b)*}) - \mu^p)^2 - (\mu(\theta^*) - \mu^p)^2],$$

where  $\hat{\theta}^{(b)*}$  denotes the estimated optimal calibration parameter setting in  $b$ th ( $b = 1, \dots, B$ ) macro-replication experiment,  $B$  is the total number of macro-replications. Similarly, the empirical PCS is computed as the frequency of correctly selecting true parameter setting, over macro-replications,

$$\widehat{\text{PCS}} = \frac{1}{B} \sum_{b=1}^B \mathbb{I}(\hat{\theta}^{(b)*} = \theta^*),$$

where  $\mathbb{I}(\cdot)$  is the indicator function.

A8. Supplementary numerical results for Section 6

Additional numerical results of Section 6.1.1 are provided in Figs. A1, A2, A3, and A4, which show EOC and PCS at steps  $n = 50, 100, 200$  and  $500$ , for different settings of the target mean  $\mu^p$ . The corresponding results for Section 6.1.2 are provided in Figs. A5 and A6. Supplementary numerical results for Section 6.2 are provided in Fig. A7.

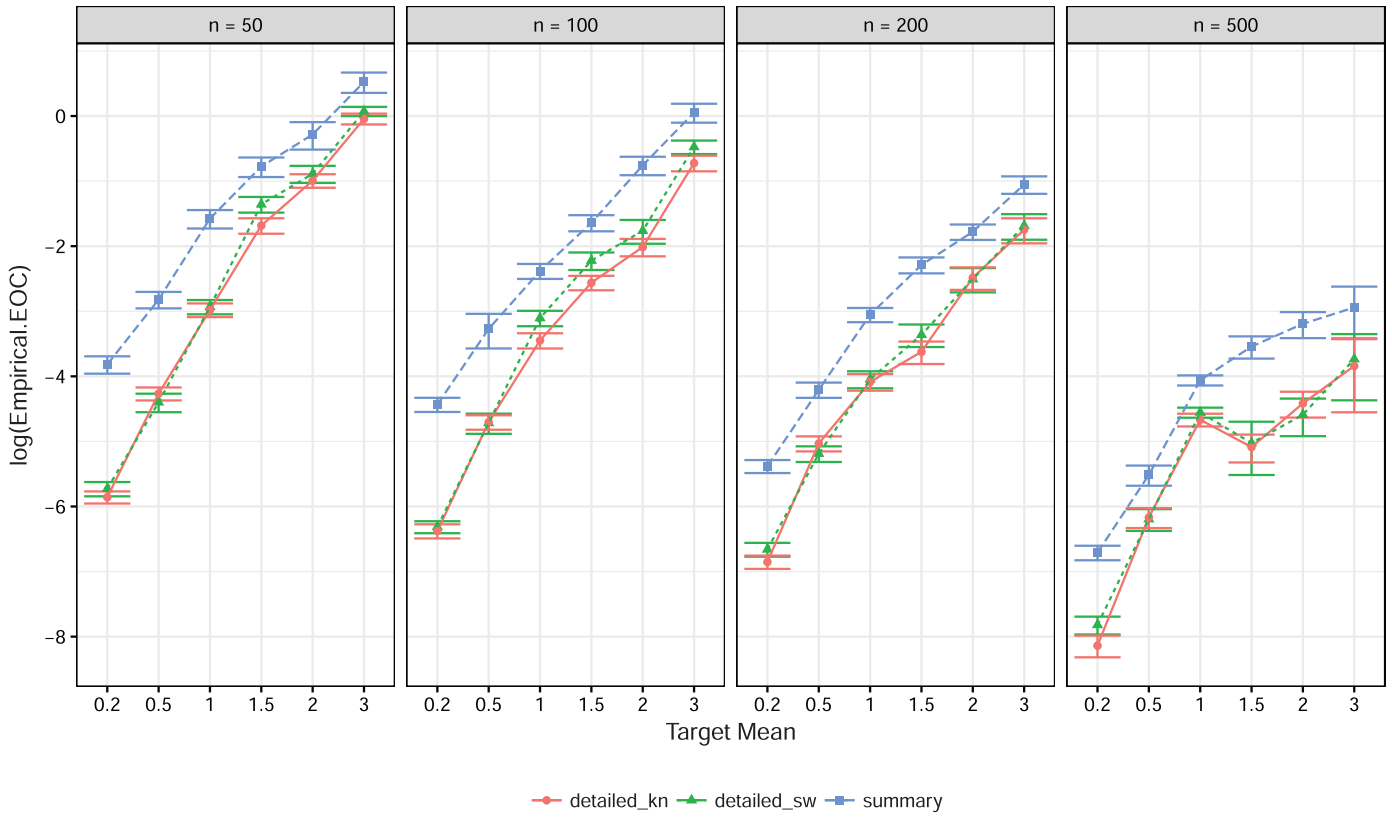


Fig. A1. Empirical EOC with 95% error bars for  $M/G/1$  queue based on 300 macro-replication.

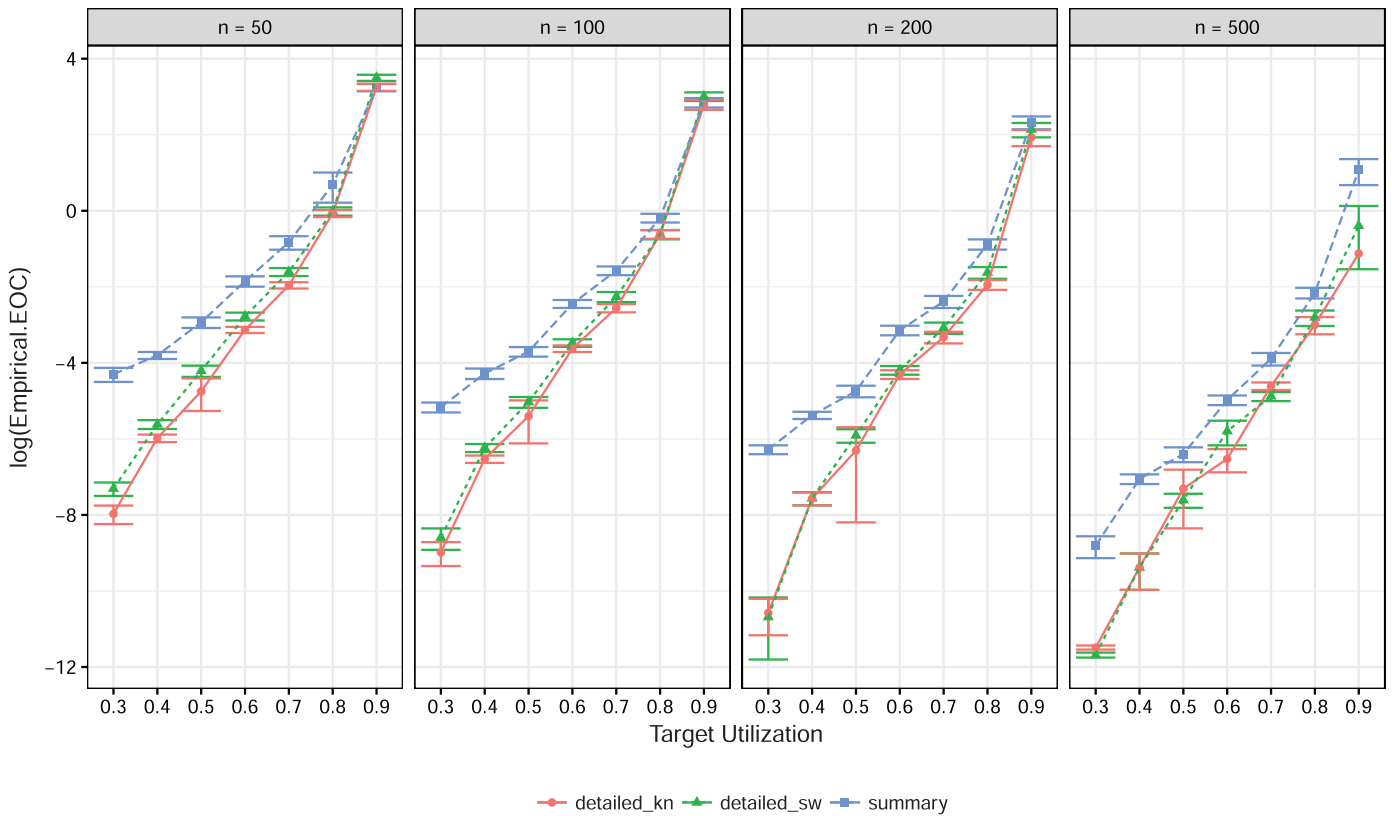


Fig. A2. Empirical EOC with 95% error bars for  $M/M/1$  queue based on 300 macro-replication.

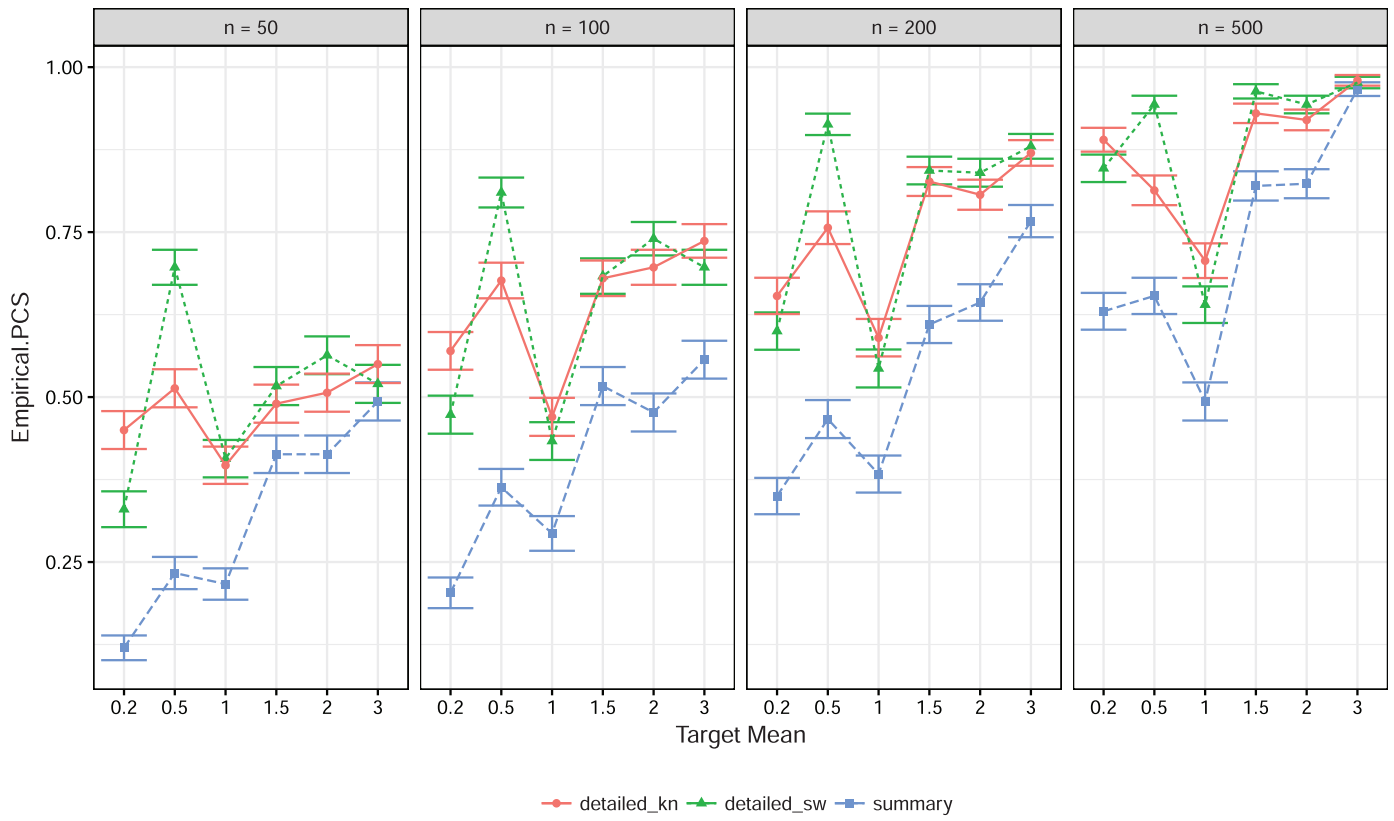


Fig. A3. Empirical PCS with 95% error bars for  $M/G/1$  queue based on 300 macro-replication.

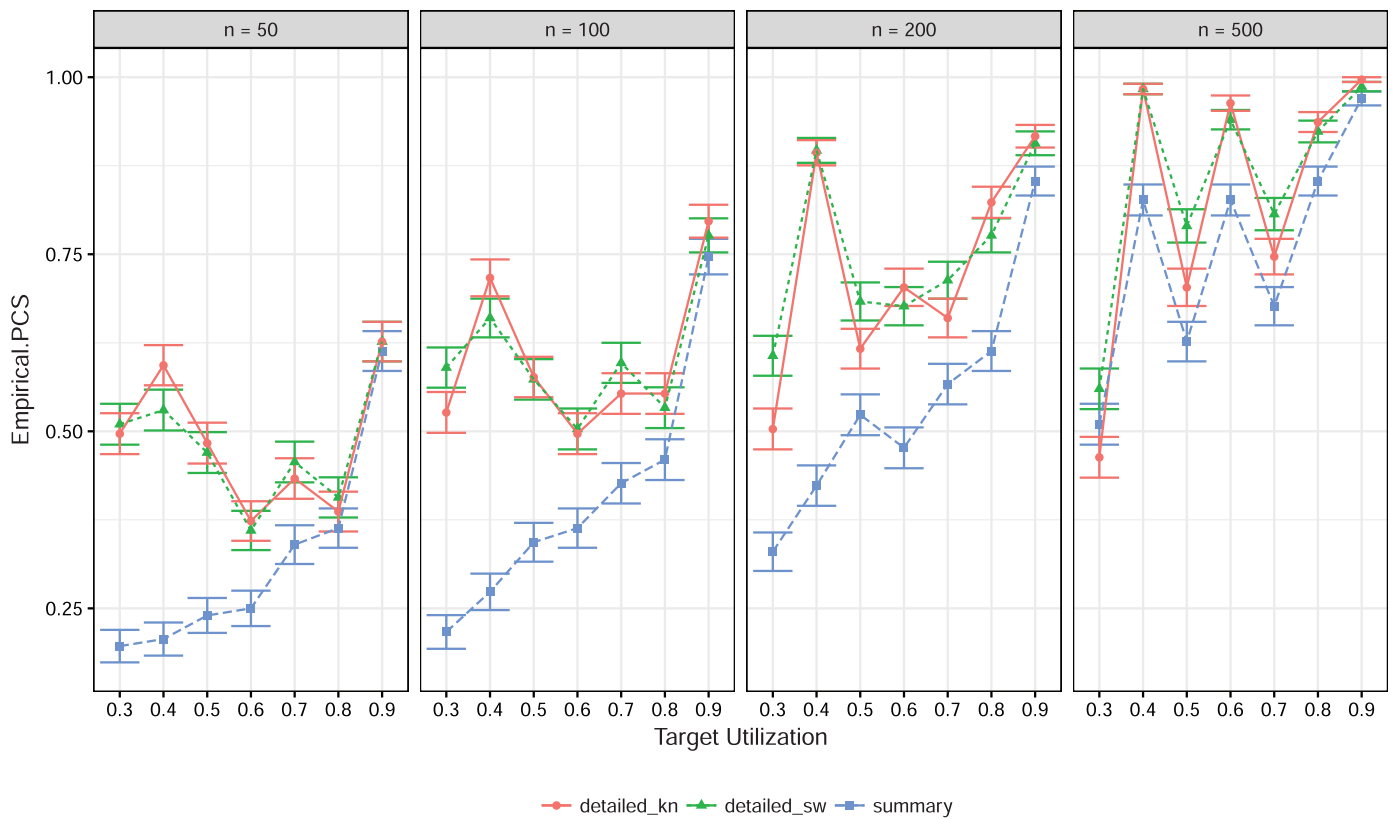


Fig. A4. Empirical PCS with 95% error bars for  $M/M/1$  queue based on 300 macro-replication.

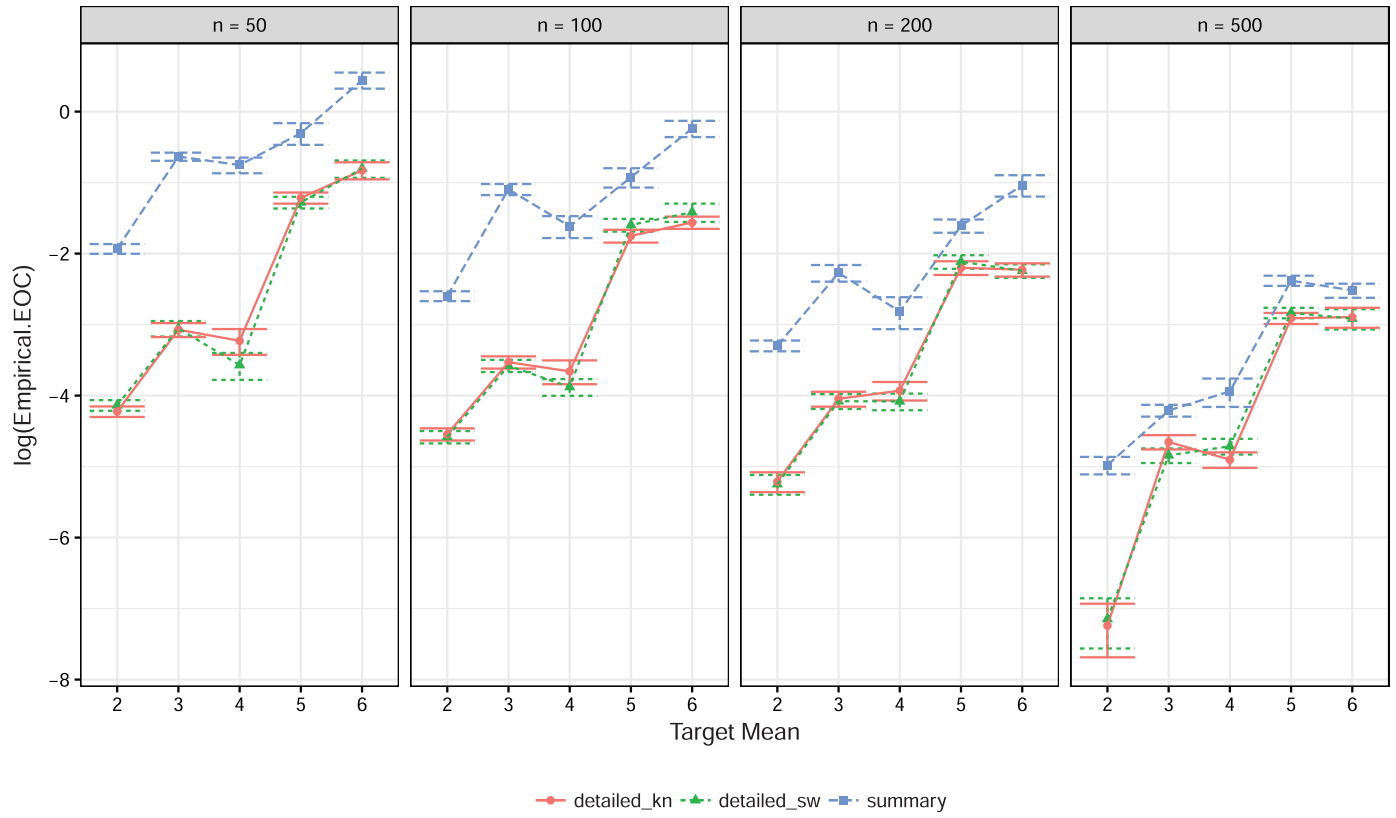


Fig. A5. Empirical EOC with 95% error bars for 3-station Jackson network based on 300 macro-replication.

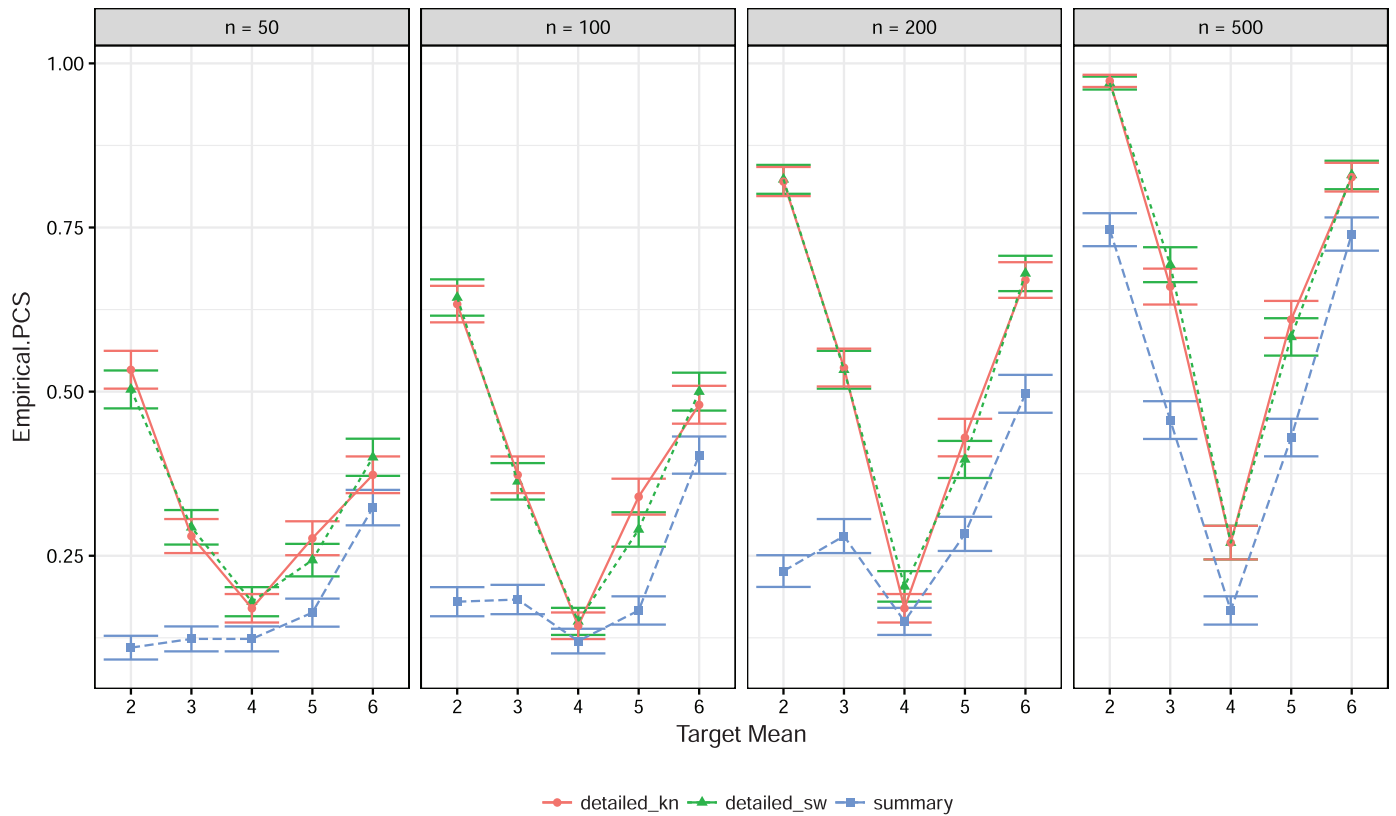
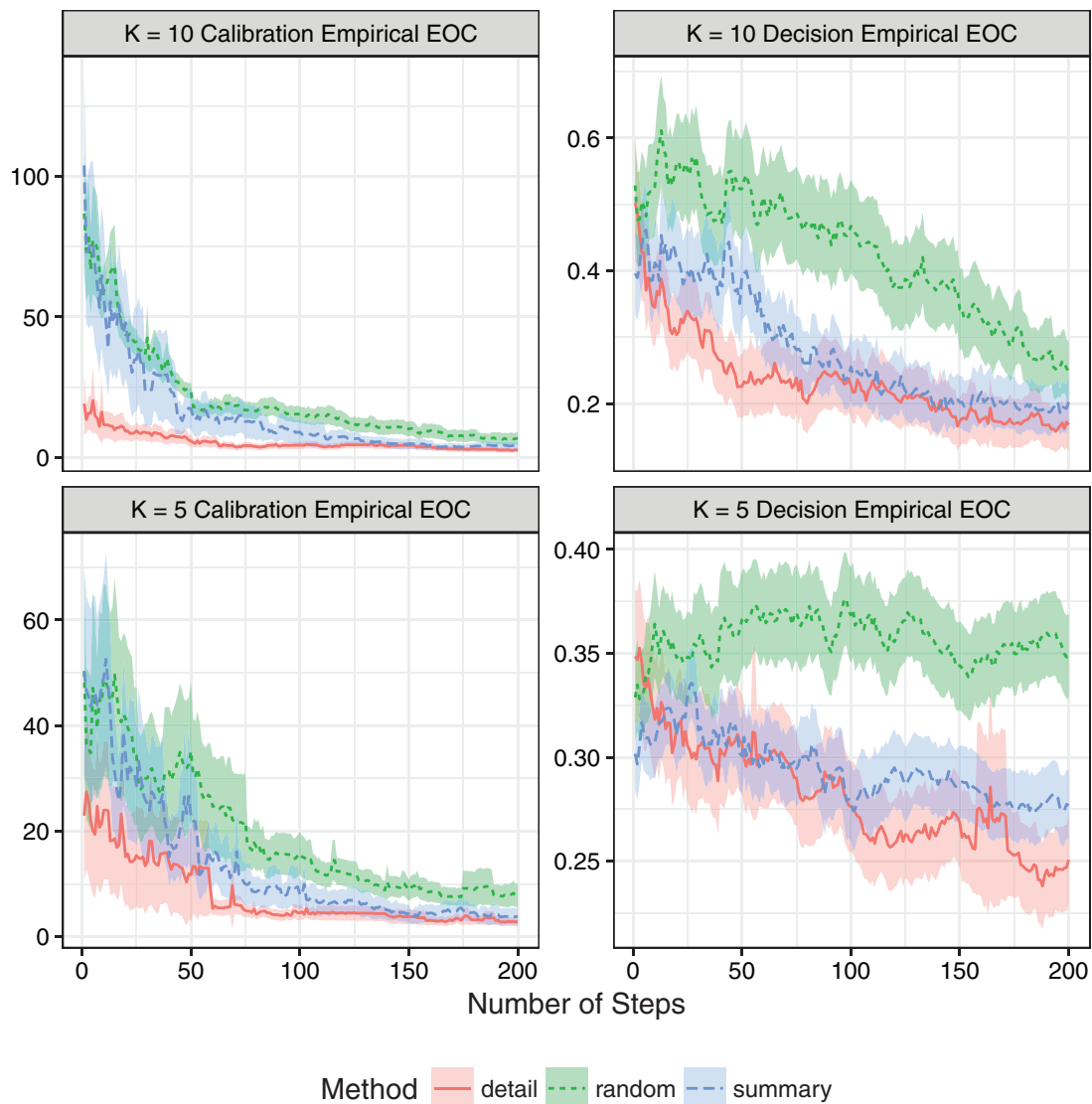


Fig. A6. Empirical PCS with 95% error bars for 3-station Jackson network based on 300 macro-replication.



**Fig. A7.** Empirical EOC of calibration and decision with 95% confidence band at each step of the 3-station Jackson network in decision and calibration process for  $K = 5$  and  $K = 10$ . The figure shows detailed approach performs the best and random approach performs the worst among the three methods.

## References

- Carnell, R. (2016). lhs: Latin hypercube samples. R package version 0.14.
- Cressie, N., & Johannesson, G. (2008). Fixed rank Kriging for very large spatial data sets. *Journal of the Royal Statistical Society: Series B (Statistical Methodology)*, 70(1), 209–226.
- Frazier, P., Powell, W. B., & Simaão, H. P. (2009). Simulation model calibration with correlated knowledge-gradients. In M. D. Rossetti, R. R. Hill, B. Johansson, A. Dunkin, & R. G. Ingalls (Eds.), *Proceedings of the 2009 winter simulation conference* (pp. 339–351). Piscataway, New Jersey: Institute of Electrical and Electronics Engineers, Inc.
- Frazier, P. I., Powell, W. B., & Dayanik, S. (2008). A knowledge-gradient policy for sequential information collection. *SIAM Journal on Control and Optimization*, 47(5), 2410–2439.
- Goeva, A., Lam, H., & Zhang, B. (2014). Reconstructing input models via simulation optimization. In A. Tolk, S. Y. Diallo, I. O. Ryzhov, L. Yilmaz, S. Buckley, & J. A. Miller (Eds.), *Proceedings of the 2014 winter simulation conference* (pp. 698–709). Piscataway, New Jersey: Institute of Electrical and Electronics Engineers, Inc.
- Gramacy, R. B., Bingham, D., Holloway, J. P., Grosskopf, M. J., Kuran, C. C., Rutter, E., et al. (2015). Calibrating a large computer experiment simulating radiative shock hydrodynamics. *The Annals of Applied Statistics*, 9(3), 1141–1168.
- Horiguchi, K., Raghavan, N., Uzsoy, R., & Venkateswaran, S. (2001). Finite-capacity production planning algorithms for a semiconductor wafer fabrication facility. *International Journal of Production Research*, 39(5), 825–842.
- Kennedy, M. C., & O'Hagan, A. (2001). Bayesian calibration of computer models. *Journal of the Royal Statistical Society: Series B (Statistical Methodology)*, 63(3), 425–464.
- Lin, Y., & Nelson, B. L. (2016). Simulation analytics for virtual statistics via k nearest neighbors. In T. M. K. Roeder, P. I. Frazier, R. Szechtman, E. Zhou, T. Huschka, & S. E. Chick (Eds.), *Proceedings of the 2016 winter simulation conference* (pp. 448–459). Piscataway, New Jersey: Institute of Electrical and Electronics Engineers, Inc.
- Luo, J., Hong, L. J., Nelson, B. L., & Wu, Y. (2015). Fully sequential procedures for large-scale ranking-and-selection problems in parallel computing environments. *Operations Research*, 63(5), 1177–1194.
- Nelson, B. L. (2016). 'some tactical problems in digital simulation' for the next 10 years. *Journal of Simulation*, 10, 2–11.
- Plumlee, M. (2017). Bayesian calibration of inexact computer models. *Journal of the American Statistical Association*, 112(519), 1274–1285.
- Plumlee, M., & Lam, H. (2016a). Fourier trajectory analysis for identifying system congestion. In T. M. K. Roeder, P. I. Frazier, R. Szechtman, E. Zhou, T. Huschka, & S. E. Chick (Eds.), *Proceedings of the 2016 winter simulation conference* (pp. 401–412). Piscataway, New Jersey: Institute of Electrical and Electronics Engineers, Inc.
- Plumlee, M., & Lam, H. (2016b). Learning stochastic model discrepancy. In T. M. K. Roeder, P. I. Frazier, R. Szechtman, E. Zhou, T. Huschka, & S. E. Chick (Eds.), *Proceedings of the 2016 winter simulation conference* (pp. 413–424). Piscataway, New Jersey: Institute of Electrical and Electronics Engineers, Inc.

- Powell, W. B., & Ryzhov, I. O. (2012). *Optimal Learning*. John Wiley and Sons.
- Qu, H., Ryzhov, I. O., Fu, M. C., & Ding, Z. (2015). Sequential selection with unknown correlation structures. *Operations Research*, 63(4), 931–948.
- Ryzhov, I. O. (2016). On the convergence rates of expected improvement methods. *Operations Research*, 64(6), 1515–1528.
- Ryzhov, I. O. (2018). The local time method for targeting and selection. *Operations Research*.
- Scott, W., Frazier, P., & Powell, W. (2011). The correlated knowledge gradient for simulation optimization of continuous parameters using gaussian process regression. *SIAM Journal on Optimization*, 21(3), 996–1026.
- Tuo, R., & Wu, C. F. J. (2016). A theoretical framework for calibration in computer models: parametrization, estimation and convergence properties. *SIAM/ASA Journal on Uncertainty Quantification*, 4(1), 767–795.
- Tuo, R., & Wu, C. J. (2015). Efficient calibration for imperfect computer models. *The Annals of Statistics*, 43(6), 2331–2352.
- Wang, B., Zhang, Q., & Xie, W. (2017). Bayesian sequential calibration using detailed sample paths. In *Proceedings of the 2017 winter simulation conference (wsc)* (pp. 1962–1973). doi:10.1109/WSC.2017.8247931.
- Whittle, P. (1954). On stationary processes in the plane. *Biometrika*, 434–449.
- Wong, R. K. W., Storlie, C. B., & Lee, T. C. M. (2017). A frequentist approach to computer model calibration. *Journal of the Royal Statistical Society: Series B (Statistical Methodology)*, 79(2), 635–648.
- Yuan, J., & Ng, S. H. (2013). An entropy based sequential calibration approach for stochastic computer models. In R. Pasupathy, S.-H. Kim, A. Tolk, R. Hill, & M. E. Kuhl (Eds.), *Proceedings of the 2013 winter simulation conference* (pp. 589–600). Piscataway, New Jersey: Institute of Electrical and Electronics Engineers, Inc.
- Yuan, J., Ng, S. H., & Tsui, K. L. (2013). Calibration of stochastic computer models using stochastic approximation methods. *IEEE Transactions on Automation Science and Engineering*, 10(1), 171–186.